A transiently expressed SK current sustains and modulates action potential activity in immature mouse inner hair cells

Walter Marcotti, Stuart L. Johnson and Corné J. Kros

School of Life Sciences, University of Sussex, Falmer, Brighton BN1 9QG, UK

From just after birth, mouse inner hair cells (IHCs) expressed a Ca^2-activated K^+ current that was reduced by intracellular BAPTA at concentrations $\geq$ 1 mM. The block of this current by nifedipine suggests the direct involvement of $Ca_v1.3$ Ca^{2+} channels in its activation. On the basis of its high sensitivity to apamin (K_D 360 pM) it was identified as a small-conductance Ca^{2+}-activated K^+ current (SK), probably SK2. A similar current was also found in outer hair cells (OHCs) from the beginning of the second postnatal week. In both cell types the appearance of the SK current coincided with their becoming responsive to acetylcholine (ACh), the main efferent neurotransmitter in the cochlea. The effect of ACh on IHCs was abolished when they were simultaneously superfused with strychnine, consistent with the presence of nicotinic ACh receptors (nAChRs). Extracellular Ca^{2+} either potentiated or blocked the nAChR current depending on its concentration, as previously reported for the recombinant $\alpha9\alpha10$ nAChR. Outward currents activated by ACh were reduced by blocking the SK current with apamin or by preventing SK current activation with intracellular BAPTA ($\geq$ 10 mM). The endogenous mobile Ca^{2+} buffer concentration was estimated to be equivalent to about 1 mM BAPTA, suggesting that in physiological conditions the SK channel is significantly activated by Ca^{2+} influx through both $Ca_v1.3$ Ca^{2+} channels and $\alpha9\alpha10$ nAChRs. Current clamp experiments showed that in IHCs the SK current is required for sustaining a train of action potentials and also modulates their frequency when activated by ACh.

(Resubmitted 29 July 2004; accepted 23 August 2004; first published online 26 August 2004)
Corresponding author C. J. Kros: School of Life Sciences, University of Sussex, Falmer, Brighton BN1 9QG, UK. Email: c.j.kros@sussex.ac.uk

In addition to the large-conductance Ca^{2+}-activated K^+ (BK) current, hair cells of various vertebrates also express a small-conductance SK current (Doi & Ohmori, 1993; Nenov *et al.* 1996*b*; Tucker & Fettiplace, 1996; Yamamoto *et al.* 1997; Yuhas & Fuchs, 1999). Three different members of the SK family have been cloned from the brain (SK1–3, Köhler *et al.* 1996), where they underlie the apamin-sensitive component of the afterhyperpolarization (mAHP) that follows an action potential (Sah & Faber, 2002). Only the SK2 channel type could be cloned from the mature cochlea (Nie *et al.* 2004), confirming previous *in situ* hybridization (rat: Dulon *et al.* 1998) and electrophysiological and immunohistochemical (mouse: Oliver *et al.* 2000) observations in OHCs. SK channels are activated, via the Ca^{2+} binding protein calmodulin (Xia *et al.* 1998), by a local increase in intracellular Ca^{2+} and are not intrinsically voltage dependent. In hair cells this increase is provided by Ca^{2+} influx into the cells through either voltage-gated Ca^{2+} channels (Tucker & Fettiplace, 1996) or $\alpha9\alpha10$ nAChRs (Elgoyhen *et al.* 2001; Maison *et al.* 2002). In the mature cochlea, the main role of SK channels is in cholinergic inhibition by the medial efferent fibres of the auditory nerve, which contact the electromotile OHCs (Guinan, 1996). Efferent inhibition of auditory hair cells is achieved by Ca^{2+} influx through nAChRs activating hyperpolarizing SK currents (Fuchs & Murrow, 1992; Evans, 1996; Glowatzki & Fuchs, 2000; Oliver *et al.* 2000). A similar inhibitory mechanism has also been described for vestibular hair cells (for a review see Guth & Norris, 1996). In addition to the inhibitory responses, slow and rapid excitation have also been described for some vestibular hair cells, associated with the activation of muscarinic ACh receptors (Guth & Norris, 1996) and nAChRs different from those containing the $\alpha9\alpha10$ subunits (Holt *et al.* 2003), respectively.

Rat IHCs respond to ACh at postnatal day 7 (P7) but no longer at P21 (Glowatzki & Fuchs, 2000) suggesting a specific role for the efferent neurotransmitter before their functional maturation that coincides with the onset of hearing at about P12 (Uziel *et al.* 1981). By contrast,

W. Marcotti and S. L. Johnson contributed equally to this work

 DOI: 10.1113/jphysiol.2004.072868

OHCs of both rat and gerbil first become sensitive to ACh from around P8 (Dulon & Lenoir, 1996; He & Dallos, 1999) when they become electromotile (He *et al.* 1994; Marcotti & Kros, 1999) and this sensitivity is maintained in adult cells. The developmental maturation of synaptic connections within the organ of Corti is likely to be influenced by the shape and frequency of spontaneous or induced action potentials of immature IHCs (Kros *et al.* 1998; Marcotti *et al.* 2003*a*), analogous to the immature retina (Shatz & Stryker, 1988; Maffei & Galli-Resta, 1990; Meister *et al.* 1991). The timing of the expression of various K^+ (Marcotti *et al.* 1999; Marcotti *et al.* 2003*a*) as well as Ca^{2+} and Na^+ (Marcotti *et al.* 2003*b*) currents leads to changes in the properties of action potentials that occur during IHC maturation. It is also conceivable that spiking activity might be influenced by extracellular events such as the release of neurotransmitters or neuromodulators onto IHCs by a transient efferent innervation (Gil-Loyzaga, 1995). In IHCs of pre-hearing rats it has been shown that superfusion of ACh reduced the frequency of action potentials (Glowatzki & Fuchs, 2000). In mouse IHCs efferent fibre endings make initial contact from around birth (Sobkowicz, 1992; Bruce *et al.* 1997, 2000) and therefore the efferent system could conceivably play a role in the modulation of spontaneous or induced action potentials from as early as P0. The aims of this paper were to investigate the biophysical properties, the development and the functions of the SK current in mouse cochlear IHCs. For comparison some experiments were also carried out in OHCs.

Methods

Tissue preparation

IHCs ($n = 248$) and OHCs ($n = 45$) were studied in acutely dissected organs of Corti from CD-1 mice (Swiss CD-1, Charles Rivers, Margate, UK) from embryonic day 14.5 (E14.5) to postnatal day 18 (P18) for IHCs and P0 to P25 for OHCs where the day of birth (P0) corresponds to E19.5. For embryonic experiments only, mice were paired overnight and checked for vaginal plugs the following morning. Assuming ovulation occurs midway through the dark cycle, the mid-point of the light cycle of the day following mating is considered to be E0.5. Adult and neonatal mice were killed by cervical dislocation and embryos by decapitation, in accordance with UK Home Office regulations.

The organs of Corti were dissected and transferred to a microscope chamber and immobilized using nylon mesh fixed to a stainless steel ring. The chamber was perfused by means of a peristaltic pump at a flow rate of about 10 ml h^{-1}, with extracellular solution composed of (mM): 135 NaCl, 5.8 KCl, 1.3 $CaCl_2$, 0.9 $MgCl_2$, 0.7 NaH_2PO_4, 5.6 D-glucose, 10 Hepes-NaOH, 2 sodium pyruvate. Amino acids and vitamins for Eagle's minimum essential medium (MEM) were added from concentrates (Invitrogen, Paisley, UK). The pH was adjusted to 7.5 and the osmolality was about 308 mosmol kg^{-1}. The organs of Corti were observed with an upright microscope (Zeiss ACM, Germany or Olympus, Japan) with Nomarski differential interference contrast optics ($\times$ 40 water immersion objectives). Only healthy-looking cells (criteria included smooth surface of the cell membrane, absence of vacuoles in the cytoplasm and lack of Brownian motion of mitochondria) with well-preserved hair bundles were investigated. The position of cells along the cochlea was recorded as fractional distance from the extreme apex. In the immature cochlea, apical-coil cells were positioned at a fractional distance between 0.16 and 0.24 and basal-coil cells between 0.83 and 0.90. Mature apical-coil cells (> P12) were positioned between 0.07 and 0.24, corresponding to an approximate frequency range of 0.9–4.2 kHz (using eqn (13) in Ehret, 1975).

Electrical recording

Whole-cell voltage-clamp recordings were performed using an EPC-8 (HEKA, Lambrecht, Germany) or an Optopatch (Cairn Research Ltd, Faversham, UK) patch-clamp amplifier. Membrane currents under voltage clamp from IHCs and OHCs were studied at room temperature (22–25°C) apart from those shown in Fig. 1 that have been recorded near body temperature (35–37°C). To obtain realistic voltage responses, all current clamp experiments were performed at 35–37°C. Patch pipettes were pulled from soda glass capillaries (Harvard apparatus Ltd, Edenbridge, UK) and electrode resistances in extracellular solution were around 2–3 MΩ. The shanks of the pipettes were coated with surf wax (Mr Zogs SexWax, Carpinteria, CA, USA) to reduce their capacitance.

The pipette filling solution for most of the current and voltage recordings contained (mM): 131 KCl, 3 $MgCl_2$, 5 Na_2ATP, 1 EGTA-KOH, 5 Hepes-KOH, 10 sodium phosphocreatine (pH 7.3, 292 mosmol kg^{-1}). For some experiments, designed to determine the possible colocalization between SK channels and either Ca^{2+} channels (Fig. 2*C*, *E* and *F*) or nAChRs (Fig. 7) in immature IHCs, different concentrations (0.1 mM, 1 mM, 10 mM and 30 mM) of the fast Ca^{2+} buffer BAPTA (Molecular Probes, Leiden, the Netherlands) or 10 mM EGTA (Fig. 7) were used instead of 1 mM EGTA (Fluka, Gillingham, UK) in the intracellular solution. When the Ca^{2+} buffer added to the intracellular solution had a concentration > 1 mM the concentration of KCl was adjusted to keep osmolality constant. From the access resistance of the electrodes (Oliva *et al.* 1988), we can estimate that the time constant of diffusion from the patch pipette to the cytoplasm for BAPTA is about 1 min.

Therefore, all currents in the presence of BAPTA were recorded after a few minutes from reaching the whole-cell configuration to allow the cytoplasm to equilibrate with the pipette solution.

In some experiments, the perforated-patch technique (Rae *et al.* 1991) was used to investigate the Ca^{2+}-dependent activation of the SK current in the presence of the endogenous Ca^{2+} buffer in immature IHCs (Figs 2*D–F* and 7*E* and *F*). For these voltage recordings the pipette filling solution contained (mM): 21 KCl, 110 potassium aspartate, 3 $MgCl_2$, 5 Na_2ATP, 1 EGTA-KOH, 5 Hepes-KOH, 10 sodium phosphocreatine (pH 7.3, 296 mosmol kg^{-1}). The antibiotic amphotericin B (Calbiochem, Nottingham, UK) was dissolved in dry dimethylsulfoxide which was diluted 1 : 500 into the above intracellular solution to a final concentration of antibiotic of 60 or 120 $\mu g\,ml^{-1}$. The patch pipette was tip-filled with the antibiotic-free solution, and back-filled with the amphotericin B solution to prevent leakage into the bath before sealing to the cell membrane.

Data acquisition was performed using pCLAMP software (Axon Instruments, Union City, CA, USA) connected to a LabMaster DMA Interface or a Digidata 1320 A. Data were filtered at 2.5 kHz (8 pole Bessel), sampled at 5 kHz and stored on computer for off-line analysis using Origin software (OriginLab, Northampton, MA, USA). For voltage-clamp experiments, current recordings were corrected offline for leak conductance (g_{leak}) usually measured around −90 mV of 1.8 ± 0.1 nS ($n = 237$, E14.5–P10) for immature IHCs and 5.3 ± 0.7 nS ($n = 8$, P12–P16) for more mature IHCs after the onset of hearing. For immature OHCs g_{leak} around −90 mV was 1.6 ± 0.2 nS ($n = 27$, P3–P7). In mature OHCs g_{leak} was measured at very hyperpolarized potentials (typically between −114 and −124 mV) at which the large $I_{K,n}$ (Marcotti & Kros, 1999) was deactivated (1.6 ± 0.2 nS, $n = 18$, P9–P25). Membrane capacitance (C_m) was 8.3 ± 0.1 pF ($n = 248$) in IHCs and 7.2 ± 0.2 pF ($n = 45$) in OHCs. In whole-cell recordings, the residual series resistance (R_s) after compensation (50–90%) was 1.9 ± 0.1 MΩ ($n = 242$, E14.5–P18, ranging from 0.5 to 7.1 MΩ) in IHCs and 2.5 ± 0.2 MΩ ($n = 45$, P3–P25, ranging from 1.0 to 6.6 MΩ) in OHCs resulting in average voltage-clamp time constants of about 15 and 19 μs, respectively. Under perforated-patch conditions, R_S after compensation (0–70%) was 10.8 ± 2.3 MΩ ($n = 6$, P8–P9, ranging from 3.8 to 20 MΩ) and the average voltage-clamp time constant was 83 μs. Membrane potentials were corrected for residual series resistance and for a liquid junction potential measured between pipette and bath solutions. The liquid junction potential was usually −4 mV for the KCl-based and −10 mV for the potassium aspartate-based intracellular solution. When the Ca^{2+} buffers in the KCl-based intracellular solution were increased to 10 or 30 mM it was −5 and −8 mV, respectively. For current-clamp experiments, offline series resistance correction was applied when the voltage drop exceeded 1 mV. When 10 or 30 mM of the Ca^{2+} buffers were used the holding potential was −85 and −88 mV, respectively. During perforated-patch recordings the holding potential was −80 or −90 mV. The holding currents were plotted as zero current unless otherwise stated.

Extracellular superfusion

The K^+ channel blocker apamin (Calbiochem) was superfused to abolish the SK current specifically. Acetylcholine and strychnine (Sigma, Gillingham, UK) were used to assess the presence of nAChRs in hair cells. The dependence of the outward K^+ current on Ca^{2+} channels was investigated by extracellular application of nifedipine (Sigma) or a Ca^{2+}-free solution containing 0.5 mM EGTA (Figs 2 and 3*A*), in which $MgCl_2$ was increased to 3.9 mM to keep membrane charge screening approximately constant (Blaustein & Goldman, 1968).

The effects of extracellular Ca^{2+} on the nAChR (Fig. 8) were investigated by the superfusion of either a Ca^{2+}-free solution (including 0.5 mM EGTA) or solutions containing different Ca^{2+} concentrations (100 μM, 500 μM, 1 mM and 5 mM). The concentration of NaCl was adjusted to keep osmolality constant. Since Mg^{2+} exerts a concentration-dependent block on the nicotinic ACh-activated current (Weisstaub *et al.* 2002), its concentration in the above solutions was kept constant at 0.9 mM, even in the Ca^{2+}-free solution. All extracellular solutions were applied through a multibarrelled pipette positioned close to the patched cell.

Statistical analysis

Statistical comparisons of means were made by the two-tailed *t* test or, for multiple comparisons, analysis of variance, usually one-way ANOVA followed by the Tukey test (Figs 2*E*, 7*E*, 8*C-E* and 9*F*). Mean values are quoted ± S.E.M. in text and figures. In Figs 2*E*, 7*E* and 8*C–E* statistically significant differences ($P < 0.05$) are indicated by an asterisk.

Results

Immature IHCs and mature OHCs express a Ca^{2+}-sensitive K^+ current

Immature IHCs exhibited, in addition to delayed rectifier K^+ currents (Marcotti *et al.* 2003*a*), a slowly activating outward current (Fig. 1: P3 and P9, indicated by arrows) that was evident when they were depolarized for a period in the order of seconds from the holding potential of −84 mV using 1 mM EGTA as the intracellular Ca^{2+} buffer

and 1.3 mM extracellular Ca^{2+}. This current was first seen around P0 in basal and P2 in apical IHCs and was no longer evident upon maturation (Fig. 1: P17). When the extracellular Ca^{2+} concentration was increased from 1.3 mM to 5 mM, this novel current was already evident using shorter (160 ms) depolarizing voltage steps ($n = 4$, P4 apical IHCs, data not shown) indicating its direct dependence on extracellular Ca^{2+}. By contrast, immature OHCs (P0–P7) did not exhibit this slowly activating current (Fig. 2*G*). When a Ca^{2+}-free solution (containing 0.5 mM EGTA) was superfused onto immature IHCs the slowly activating outward current was selectively and reversibly abolished (Fig. 2*A*), providing further evidence for its Ca^{2+} sensitivity. This current was also blocked (Fig. 2*B*) when nifedipine (30 or 50 μM) was superfused onto apical IHCs (P9, $n = 5$) implicating the involvement of L-type Ca^{2+} channels in its activation. The Ca^{2+}- and nifedipine-insensitive current (Fig. 2*A* and *B*, red traces) exhibits a decay time course similar to that of the total outward K^+ current expressed by embryonic IHCs, i.e. before the appearance of the slowly activating current (Fig. 1, E18.5), and by immature (P0–P7) OHCs (Fig. 2*G*, black traces). The maximum size of the Ca^{2+}-sensitive K^+ current in apical IHCs, measured at the steady state (4 s) around −20 mV, was 981 ± 223 pA ($n = 4$, P3 and P7).

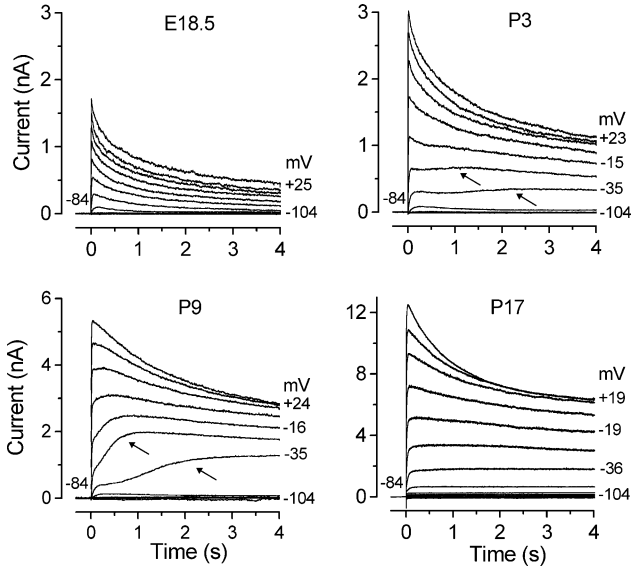

Figure 1. Development of the slowly activating outward current in IHCs

Membrane currents were recorded from apical IHCs at different developmental stages. Currents were elicited by 4 s depolarizing voltage steps in 10 mV nominal increments from −104 mV starting from the holding potential of −84 mV. Actual test potentials reached are shown by some of the traces. The arrows point to the slowly activating component, at two different membrane potentials. Note the different scales used for the current size. In this and in the following figures current recordings are single traces. E18.5: C_m 6.8 pF; R_s 1.4 MΩ; g_{leak} 1.8 nS. P3: C_m 8.1 pF; R_s 1.8 MΩ; g_{leak} 1.8 nS. P9: C_m 10.5 pF; R_s 1.1 MΩ; g_{leak} 1.0 nS. P17: C_m 9.3 pF; R_s 0.8 MΩ; g_{leak} 4.0 nS. All recordings were obtained at body temperature.

Since this novel K^+ current was abolished in the absence of extracellular Ca^{2+}, we investigated its sensitivity to cytosolic Ca^{2+} using different concentrations of the fast Ca^{2+} buffer BAPTA (Neher, 1998). Figure 2*C* shows current recordings from apical IHCs (P9) using 0.1 mM, 1 mM or 30 mM BAPTA as the internal Ca^{2+} buffer instead of 1 mM EGTA. The IHCs buffered with 0.1 mM and 1 mM BAPTA, but not that with 30 mM BAPTA, showed the slowly activating outward K^+ current (arrows) that was completely and reversibly abolished during superfusion of a Ca^{2+}-free solution (red traces). Increasing the BAPTA concentration from 0.1 to 1 mM slowed the activation of the Ca^{2+}-sensitive current, suggesting that the kinetics of the current reflect the time course of the change in intracellular Ca^{2+} (Tucker & Fettiplace, 1996). To determine the contribution of this Ca^{2+}-sensitive current under endogenous Ca^{2+} buffering conditions and in the presence of 1.3 mM extracellular Ca^{2+}, recordings from five P8–P9 IHCs were obtained using the perforated-patch technique. Figure 2*D* shows that the slowly activating current was evident in the presence of the native mobile buffer and that it was abolished during superfusion of a Ca^{2+}-free solution. The amplitudes of the Ca^{2+}-sensitive K^+ current in P8–P9 apical IHCs ($n = 23$), measured near the beginning (100 and 200 ms) and at the end (4 s) of the voltage step, using whole-cell (intracellular 1 mM EGTA or different BAPTA concentrations) or perforated-patch recording are shown in Fig. 2*E*. Relative to recordings with 1 mM EGTA, the size of the Ca^{2+}-sensitive K^+ current, measured near −26 mV and near the beginning of the voltage step, was significantly ($P < 0.001$) reduced in the presence of 1 mM or higher BAPTA concentrations but not by 0.1 mM BAPTA. The current amplitude was also reduced ($P < 0.01$) when recorded under perforated-patch conditions. However, 10 mM or 30 mM BAPTA was needed to reduce significantly ($P < 0.001$) the amplitude of the Ca^{2+}-sensitive current when measured at 4 s. These results suggest that during long-lasting voltage steps (> 400 ms) increasingly higher BAPTA concentrations are required to buffer the larger influx of Ca^{2+} flowing through voltage-gated Ca^{2+} channels. The effects of BAPTA were evident within a minute from reaching the whole-cell configuration. An approximate concentration of the endogenous mobile Ca^{2+} buffer, expressed as an equivalent BAPTA concentration, can be estimated by comparing the size of the Ca^{2+}-sensitive current in the perforated-patch recordings with that obtained using different intracellular BAPTA concentrations (Fig. 2*E*). The amplitude of the Ca^{2+}-sensitive current, measured at 100 or 200 ms in perforated-patch recordings, corresponds to that which would be obtained in about 0.7 mM BAPTA (Fig. 2*F*). When measured at 4 s native Ca^{2+} buffering was more efficient, equivalent to about 4 mM BAPTA, possibly

reflecting the recruitment of additional buffers or Ca^{2+} sequestration (Tucker & Fettiplace, 1996).

Consistent with the absence of the slowly activating current in immature OHCs (Fig. 2*G*, black traces) the total outward K^+ current was unaffected when cells (P3–P6, $n = 6$) were superfused with a Ca^{2+}-free solution (Fig. 2*G*, red traces). It is worth mentioning that in one apical P6 OHC a very small Ca^{2+}-sensitive current (about 30 pA) was isolated. By P9 all OHCs exhibited a similar slowly activating Ca^{2+}-sensitive current (109 ± 21 pA, measured at 4 s near −15 mV, P9 and P12, $n = 5$, data not shown), suggesting that a similar current to that expressed in immature IHCs is present in OHCs from the beginning of the second postnatal week.

The Ca^{2+}-activated K^+ current is carried by SK channels

A selective reduction of the Ca^{2+}-activated K^+ current was also obtained when immature IHCs were superfused with apamin, a selective blocker of SK channels (Sah & Faber, 2002). Extracellular application of 300 nM apamin (Fig. 3*A*, blue traces) selectively abolished the slowly activating outward current expressed in immature IHCs (P7, $n = 3$). To test whether the Ca^{2+}-sensitive component of the outward K^+ current was completely abolished by apamin, the same IHCs were additionally superfused with a Ca^{2+}-free solution also containing 300 nM apamin. Figure 3*A* (red traces) shows that a Ca^{2+}-free solution did not further reduce the total outward K^+ current.

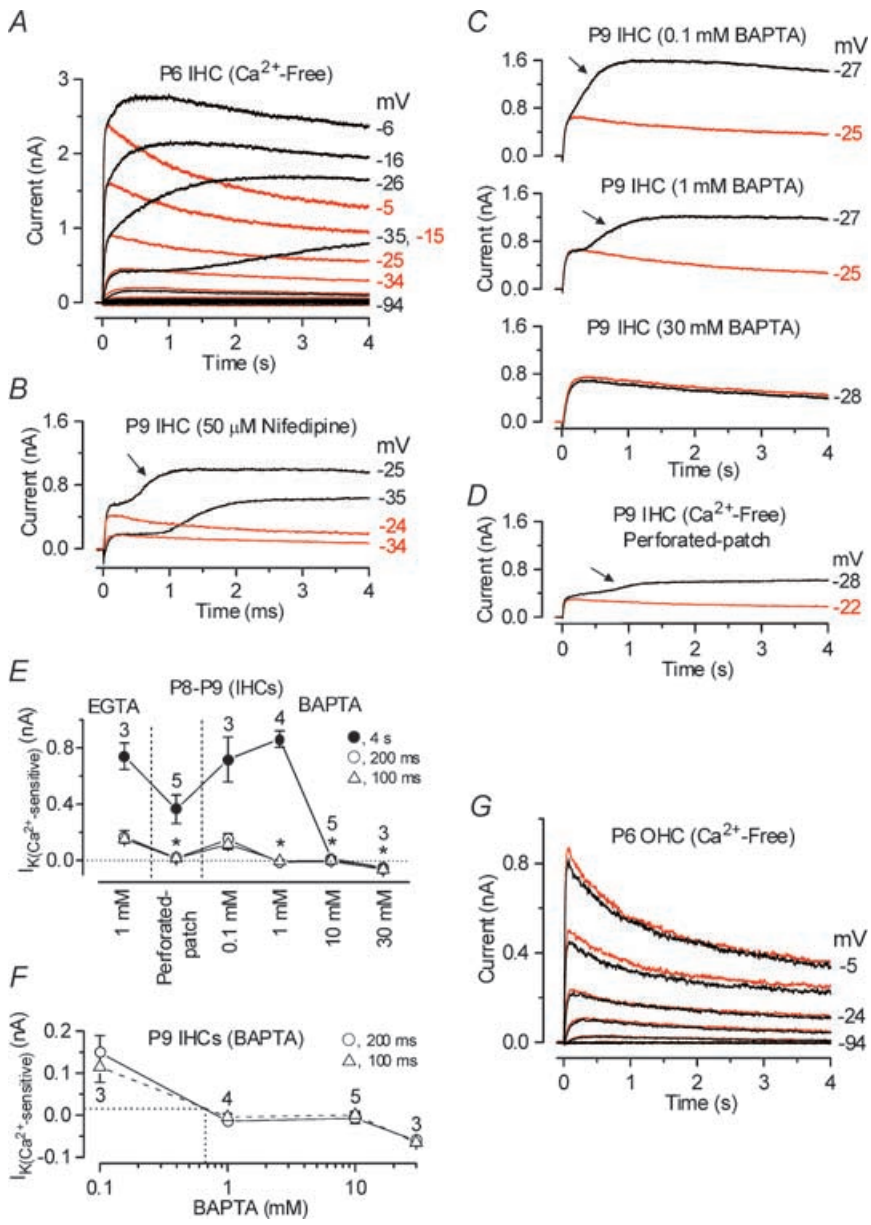

Figure 2. The slowly activating outward current of immature IHCs is Ca^{2+} sensitive
A, membrane currents obtained from a P6 apical IHC before (black traces) and during (red traces) superfusion of a Ca^{2+}-free solution. Currents were elicited by 4 s depolarizing voltage steps in 10 mV nominal increments from −94 mV starting from the holding potential of −84 mV. C_m 8.4 pF; R_s 1.0 MΩ; g_{leak} 1.1 nS. *B*, current recordings from a P9 apical IHC before (black traces) and during (red traces) superfusion of 50 μM nifedipine. Holding potential −84 mV. C_m 9.0 pF; R_s 1.5 MΩ; g_{leak} 2.8 nS. *C*, membrane currents from apical IHCs (P9) in the presence of different BAPTA concentrations before (black traces) and during (red traces) superfusion of a Ca^{2+}-free solution. 0.1 mM BAPTA: C_m 8.6 pF; R_s 2.5 MΩ; g_{leak} 2.5 nS. 1 mM BAPTA: C_m 9.4 pF; R_s 1.4 MΩ; g_{leak} 3.6 nS. 30 mM BAPTA: C_m 8.6 pF; R_s 1.1 MΩ; g_{leak} 3.1 nS. *D*, currents recorded from a P9 IHC under perforated-patch conditions before (black trace) and during (red trace) superfusion of a Ca^{2+}-free solution. C_m 8.0 pF; R_s 13 MΩ; g_{leak} 1.8 nS. *E*, amplitude of the Ca^{2+}-sensitive K^+ current measured near −26 mV and at 100 ms, 200 ms and 4 s either in the presence of 1 mM EGTA, under perforated-patch conditions or using different BAPTA concentrations in the intracellular solution. Numbers of cells are shown in the panel. *F*, size of the Ca^{2+}-sensitive outward K^+ current as a function of BAPTA concentration (data as in *E*). The equivalent BAPTA concentration for the endogenous buffer is estimated by the dotted lines. *G*, current recordings from a P6 apical OHC before (black traces) and during (red traces) superfusion of a Ca^{2+}-free solution. Recording conditions as in *A*. C_m 6.4 pF; R_s 1.6 MΩ; g_{leak} 1.7 nS.

Apamin proved to be a very effective blocker of the SK current in apical IHCs with a K_D of 360 pM (Fig. 3*B*). Although the apamin-sensitive current could be most clearly seen using long lasting voltage steps (Fig. 3*A*), its presence has been demonstrated in immature IHCs during shorter voltage steps in the order of 100 ms when all other K^+ currents were blocked (Marcotti *et al.* 2003*b*). A selective block of the Ca^{2+}-sensitive current by apamin (300 nM, P13–P17, $n = 3$) was also observed in mature OHCs (data not shown). The effect of apamin was very difficult to wash out completely and therefore after each application of the toxin the

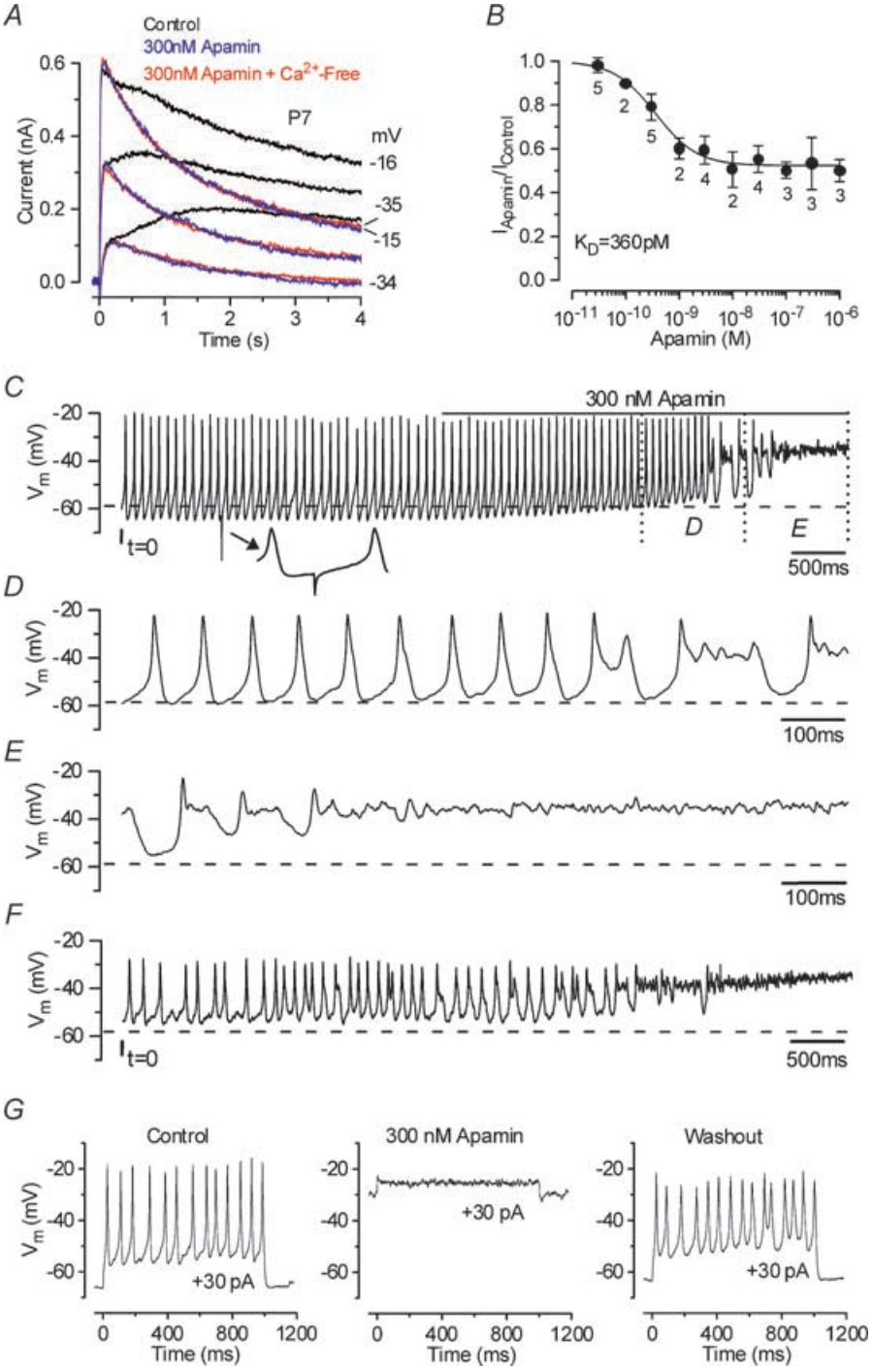

Figure 3. Apamin blocks the Ca^{2+}-sensitive current and disrupts action potential trains
A, membrane currents elicited from a P7 apical IHC before and during superfusion of 300 nM apamin (black and blue traces, respectively) and when a Ca^{2+}-free solution containing 300 nM apamin (red traces) was applied. Current recordings are in response to 4 s voltage steps in 10 mV increments from a holding potential of −84 mV. For clarity only some of the traces are shown. C_m 8.7 pF; R_s 1.4 MΩ; g_{leak} 3.3 nS. *B*, dose–response curve for the block of the outward K^+ currents by apamin, measured at 4 s at a membrane potential near −20 mV. IHCs were superfused with a range of concentrations of apamin (between 30 pM and 1 μM), which blocked the SK current. Logistic curve: $I_{apamin} = I_{res} + (I_{control} - I_{res})/(1 + ([D]/K_D)^{n_H})$ fitted with half-blocking concentration $K_D = 360 \pm 118$ pM and n_H (Hill coefficient) $= 1.1 \pm 0.4$. $[D]$ is the drug concentration and I_{res} is the residual current that remains in the presence of apamin. *C*, continuous recording of voltage responses induced by a 30 pA depolarizing current from the resting potential (−59 mV), from an apical P5 IHC at 37°C. The line above the voltage responses indicates the period of apamin application. The total duration of the recording is 7 s. The small inset below the top trace shows a spontaneous hyperpolarizing transient (see Results). *D* and *E*, expanded versions of the last 2 s of recording from panel *C*. *F*, voltage responses elicited by a steady 30 pA depolarizing current obtained from the same cell shown in *C*–*E* after 60 s of washout with apamin-free extracellular solution and no current injection. C_m 7.0 pF; R_s 7.0 MΩ; g_{leak} 3.8 nS. *G*, voltage responses from a P7 apical IHC to 30 pA depolarizing current steps before, during and after the superfusion of 300 nM apamin. The recordings in the control and in the presence of apamin are separated by about 30 s while the washout was recorded after 90 s from the start of the application of an apamin-free solution. V_m −66 mV; C_m 9.1 pF; R_s 6.4 MΩ; g_{leak} 2.5 nS. All voltage responses in this and following figures are single traces.

preparation was discarded. Although the SK current expressed in hair cells is thought to be activated by Ca^{2+} flowing through nAChRs (Elgoyhen *et al.* 2001) our results (Fig. 2*A* and *B*: Ca^{2+} and nifedipine sensitivity) show that SK channels can also be activated by Ca^{2+} influx through L-type Ca^{2+} channels containing the $Ca_v1.3$ (α1D) subunit, known to be present in mouse cochlear hair cells (Platzer *et al.* 2000; Marcotti *et al.* 2003*b*; Michna *et al.* 2003).

Blocking the SK channels impedes IHC action potential activity

Immature IHCs can generate Ca^{2+}-dependent action potentials spontaneously or in response to the injection of small depolarizing currents from the resting potential (Marcotti *et al.* 2003*b*). The shape and the frequency of these action potentials are specifically modulated by different conductances expressed during development in immature IHCs (Marcotti *et al.* 1999, 2003*a*,*b*). To determine whether the SK current also affects the IHC voltage responses, eight cells were superfused with a fully blocking concentration of apamin (100–300 nM) under current clamp using short (1 s) and long-lasting (up to 15 s) recordings. From the resting membrane potential, when a depolarizing current step of 30 pA (Fig. 3*C* and *G*, left panel) was applied to apical IHCs repetitive action potentials were elicited. The inset in Fig. 3*C* (indicated by the arrow) shows a spontaneous hyperpolarizing transient on an expanded time scale that has been previously attributed to inhibitory post-synaptic potentials (IPSPs) (Glowatzki & Fuchs, 2000). These small spontaneous hyperpolarizing transients were evident in 28% of immature IHCs (P2–P12, 26 out of 94 IHCs investigated) and they sometimes prolonged the interspike interval. Application of 300 nM apamin gradually abolished the evoked action potentials in all cells investigated (Fig. 3*C*–*E*) by progressively reducing the extent of repolarization of the IHCs after an action potential upstroke, finally resulting in a steady depolarization. Before action potential activity ceased an increase in the firing frequency was observed in some cases (e.g. from 12 to 15 Hz in Fig. 3*C*). Recordings using shorter current steps show that in the presence of apamin the cells remained depolarized in between steps, again failing to produce action potentials (Fig. 3*G*, middle panel). A fully blocking concentration of apamin (300 nM) abolished action potentials even for large depolarizing current steps (up to +100 pA tested). Therefore it appears that the delayed rectifier K^+ current, $I_{K,neo}$, alone is not sufficient to maintain repetitive spikes, most likely due to its steady-state inactivation that occurs with depolarizing voltage steps (Marcotti *et al.* 2003*a*). After washout (Fig. 3*F* and *G*, right panel), although IHCs were once more capable of firing action potentials they did not usually regain the ability of producing a sustained regular train of repetitive spikes, probably due to apamin being difficult to remove completely.

The developmental onset of ACh sensitivity differs between IHCs and OHCs

Since IHCs do respond to ACh at P7 (rat: Glowatzki & Fuchs, 2000) we investigated whether the onset of their sensitivity to ACh matched the appearance of the SK current just after birth. A typical example of the effect of ACh on an apical IHC (P8) is shown in Fig. 4*A*–*E*. The ACh-activated current (Fig. 4*C*) was obtained by subtracting the control currents (Fig. 4*A*) from the currents in the presence of 100 μM ACh (Fig. 4*B*). During superfusion of ACh the holding current measured at −84 mV (Control: -10 ± 2 pA, $n = 11$) rapidly became more negative (100 μM ACh: -462 ± 73 pA, $n = 11$, $P < 0.001$) and then, in the continued presence of ACh, it slowly (in the order of 10 s) and partially relaxed back to a value of -330 ± 51 pA ($n = 11$). This is likely to be due to the desensitization of nAChRs known to occur in both native (Fuchs & Murrow, 1992; Housley *et al.* 1992; Dulon & Lenoir, 1996; Evans, 1996) and recombinant $\alpha9\alpha10$ (Weisstaub *et al.* 2002) nAChRs. As shown in Fig. 4*C*, ACh evoked an instantaneous current that declined with time, reaching a steady-state level after about 80 ms, during both hyperpolarizing and depolarizing voltage steps from the holding potential of −84 mV. The effect of ACh on IHCs was rapid and completely reversible.

The current relaxation observed during depolarizing voltage steps has been previously described, using a similar voltage protocol, in guinea-pig OHCs and is likely to be due to a reduced driving force for Ca^{2+} with depolarization, indicating the presence of a Ca^{2+}-activated K^+ current (Evans, 1996). In contrast, the current decline observed during hyperpolarizing voltage steps relates to the presence of nAChRs themselves since it was still present when the SK channels were either blocked by apamin (Fig. 6*C*) or prevented from activating using either high (10 or 30 mM) intracellular BAPTA concentrations (Fig. 7*C*) or a Ca^{2+}-free extracellular solution (Fig. 8*A*, top left panel). Although nAChR desensitization can cause a time-dependent reduction in the current flowing through the nAChRs (Fuchs & Murrow, 1992; Housley *et al.* 1992; Dulon & Lenoir, 1996; Evans, 1996), it is unlikely that this mechanism is responsible for the current decline seen at hyperpolarized potentials for a number of reasons. First of all, the decay time course of the hyperpolarized ACh-activated current (Fig. 4*C*) appears to be faster than that of desensitization, which was in the order of seconds (Housley *et al.* 1992; Dulon & Lenoir, 1996; Evans, 1996; Glowatzki & Fuchs, 2000). Second, repetitive hyperpolarizing voltage steps during the continuous superfusion of ACh elicited currents of similar

amplitude (data not shown). A possible explanation for the current decline is a voltage-dependent block of nAChRs by extracellular Ca^{2+} (see below). The steady-state (measured at 160 ms) and the instantaneous *I–V* curves for the control current, the current in the presence of 100 μM ACh and the ACh-activated current are shown in Fig. 4*D* and *E*, respectively. The steady-state ACh-activated current is bell shaped, peaking at −27 mV (818 ± 70 pA, $n = 11$, P7–P10) and then declining at more depolarized values, as previously described for the same current in other hair cell types (Fuchs & Murrow, 1992; Dulon & Lenoir, 1996; Evans, 1996; Nenov *et al.* 1996*a*), again due to a reduced driving force for Ca^{2+}. The reversal potential of the ACh-activated current, measured from either the steady-state or the instantaneous *I–V* curves (Fig. 4*D* and *E*), was −73 mV (P7–P10), close to the K^+ equilibrium potential under our experimental conditions ($E_K = -83$ mV, 23°C) indicating that this current is mainly a K^+ current.

The sensitivity of IHCs to ACh during development was investigated by measuring the steady-state slope conductance of the total current, around the holding potential of −84 mV (Fig. 4*D*), before and during the superfusion of 100 μM ACh (apical IHCs, range P1–P16). Figure 5*A* shows that IHCs are transiently sensitive to ACh during immature stages of development. Immature apical IHCs begin to respond to ACh from just after birth, thus matching the appearance of the SK current in these cells. Although at P2 the effect of ACh on the steady-state conductance was very small (Fig. 5*A*), the holding current measured at −84 mV became significantly ($P < 0.05$) more negative in the presence of ACh (Control: −8 pA; 100 μM ACh: −22 pA; $n = 4$). Up to about P9 the slope conductance increased progressively in the presence of ACh. After that it gradually declined and by P14 the extracellular application of ACh had little effect suggesting that the nAChRs are no longer functional in mature IHCs.

When 100 μM ACh was superfused onto early postnatal apical OHCs (P4, $n = 4$), using the same recording conditions as Fig. 4*A* and *B*, no clear changes in the currents were observed (data not shown). Similar results were also obtained at P6 ($n = 5$) although a significant ($P < 0.05$) increase of the holding current was observed (control: −93 pA; 100 μM ACh: −114 pA). From the beginning of the second postnatal week the ACh-activated current, measured as steady-state slope conductance at the holding potential of −84 mV as for IHCs (Fig. 5*A*), was clearly present in all OHCs investigated (Fig. 5*B*). Contrary to IHCs, the sensitivity to the efferent neurotransmitter did not decline with OHC maturation, consistent with previous observations in rat and gerbil OHCs (Dulon & Lenoir, 1996; He & Dallos, 1999). It is worth noting that the increase in steady-state slope conductance observed in control conditions from around P9 in OHCs (Fig. 5*B*) is due to the expression of $I_{K,n}$ which

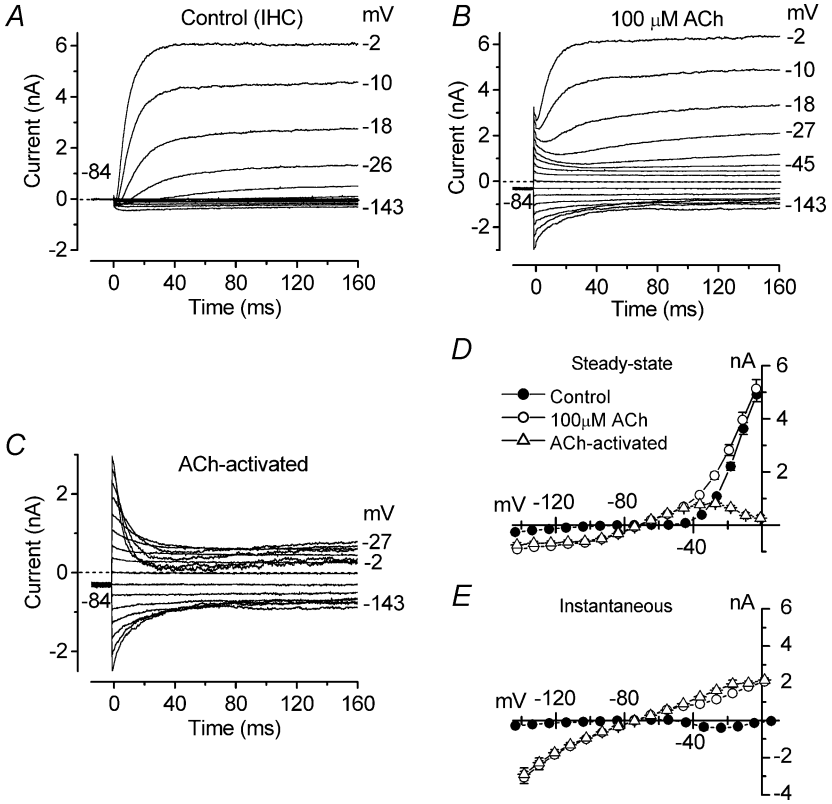

Figure 4. Effects of ACh on immature IHCs
A and *B*, membrane currents recorded from an apical P8 IHC before (*A*) and during (*B*) superfusion of 100 μM ACh in response to a series of voltage steps from −143 mV to more positive potentials in 10 mV nominal increments (160 ms in duration) from the holding potential of −84 mV. *C*, ACh-activated current obtained by subtracting the control current (*A*) from the current in the presence of 100 μM ACh (*B*). Dotted lines indicate zero current. Holding current (I_{hold}) in *A* is −6 pA, in *B* −295 pA. C_m 7.7 pF; R_s 2.3 MΩ; g_{leak} 1.3 nS. *D* and *E*, average steady-state (*D*) and instantaneous (*E*) *I–V* curves for the current recorded before and during superfusion of 100 μM ACh and the ACh-activated current ($n = 11$, P7–P10).

is about 50% active at −84 mV (Marcotti & Kros, 1999). $I_{K,n}$ is also expressed in IHCs but is smaller than in OHCs and only starts to appear from around the onset of hearing at about P12 (Marcotti *et al.* 2003*a*) contributing, together with $I_{K,f}$ (Marcotti *et al.* 2004), to the increase in the slope conductance from P12 (Fig. 5*A*, filled circles).

ACh responses are mediated by the colocalization of nAChRs and SK channels

To confirm the presence of nAChRs in immature IHCs we superfused apical cells ($n = 12$, P3–P7) with 70 or 100 μM ACh with and without 1 μM strychnine, a known antagonist of both the homomeric $\alpha9$ and the heteromeric $\alpha9\alpha10$ receptors (Elgoyhen *et al.* 1994, 2001). Figure 6*A* shows an example of membrane currents from a P3 IHC in control conditions, in the presence of 70 μM ACh and during the simultaneous superfusion of 70 μM ACh and 1 μM strychnine. When ACh was superfused alone (red traces), depolarizing and hyperpolarizing voltage steps from the holding potential of −84 mV elicited an instantaneous outward and inward current, respectively. In the presence of strychnine (blue traces) the effects of ACh were abolished suggesting the direct involvement of $\alpha9$ or $\alpha9\alpha10$ nAChRs. The block of the ACh-activated current by strychnine can be better appreciated from the steady-state *I–V* curves shown in Fig. 6*B*. We examined the involvement of SK channels in the ACh responses by the combined superfusion of 100 μM ACh and 300 nM apamin. As shown in Fig. 6*C* and *D* (P9 apical IHC) the simultaneous superfusion of ACh and apamin onto immature IHCs inhibited the additional outward current that activated near −26 mV when ACh was applied alone (Fig. 6*A*, arrowhead), showing that SK channels are directly involved in ACh responses. The large inward relaxing current remaining in the presence of apamin (Fig. 6*C*, arrowhead) is likely to be due to cations entering the cell through nAChRs activated by ACh. The same effects were seen in two additional P7 IHCs.

The distance between nAChRs and SK channels was investigated by recording membrane currents before and during superfusion of 100 μM ACh when the fast Ca^{2+} buffer BAPTA was used instead of EGTA in the intracellular solution (Naraghi & Neher, 1997). In the presence of 0.1 mM BAPTA (Fig. 7*A* and *B*) the superfusion of 100 μM ACh onto a P9 IHC activated instantaneous inward and outward currents (Fig. 7*A*) similar to those observed when 1 mM EGTA was used (Fig. 4*B*). When BAPTA was increased to 10 mM, ACh still produced a large inward current that relaxed back during hyperpolarizing voltage steps, but had no effect on the outward current (Fig. 7*C* and *D*), similar to when the SK channels were blocked by apamin (Fig. 6*C* and *D*). With 1 mM BAPTA only a partial reduction of the outward K^+ current was seen (data not shown). Block of the ACh-activated SK current by BAPTA (5 or 10 mM) has previously been reported in short (outer) hair cells of the chick (Fuchs & Murrow, 1992) and guinea-pig OHCs (Evans, 1996). Figure 7*E* shows the size of the isolated steady-state (at 160 ms) ACh-activated currents obtained by subtracting the control currents from the currents in the presence of 100 μM ACh. Currents were measured at a membrane potential near −26 mV, a value corresponding to the peak outward ACh-activated current, using the following experimental conditions: 1 mM and 10 mM EGTA in the intracellular solution (as in Fig. 4*C* for 1 mM EGTA), 1 mM EGTA with the simultaneous superfusion of 300 nM apamin, perforated-patch recording and four different intracellular BAPTA concentrations. When 300 nM apamin was applied or the intracellular solution contained 10 or 30 mM BAPTA, the superfusion of 100 μM ACh did not elicit any significant outward K^+ current. Compared with 1 mM EGTA, the size of the ACh-activated current was not significantly different when whole-cell recordings were obtained using 0.1 mM BAPTA, 1 mM BAPTA or 10 mM EGTA, or when perforated-patch was used. These results suggest that the SK current was effectively uncoupled from the nAChRs when 10 mM or higher BAPTA concentrations were used. The amplitude of the ACh-activated SK

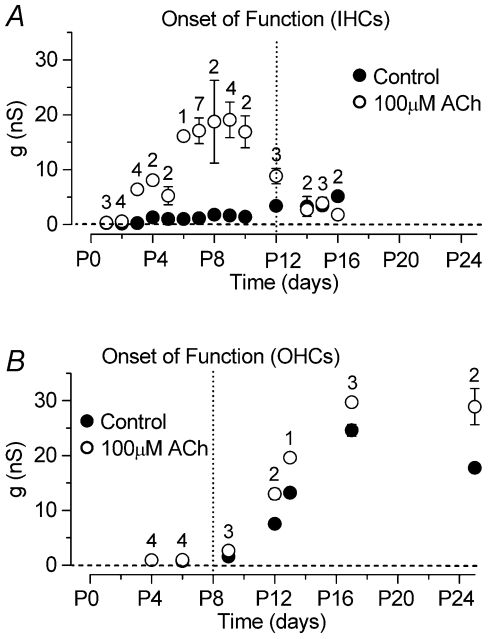

Figure 5. Development of the ACh-activated current in apical-coil IHCs and OHCs

A, steady-state slope conductance measured around −84 mV before and during superfusion of 100 μM ACh as a function of IHC development. Note that the expression of the ACh-activated current is mainly restricted to immature stages of development. *B*, steady-state slope conductance in OHCs measured using the same experimental conditions as in *A*. Dotted vertical lines indicate onset of mature function for both cell types.

current during perforated-patch recording points to an endogenous buffer concentration equivalent to 1.1 mM BAPTA (Fig. 7*F*), a value close to that obtained when the SK current activated by Ca^{2+} influx through the $Ca_v1.3$ Ca^{2+} channels was investigated (0.7 mM, Fig. 3*F*).

ACh activates $\alpha9\alpha10$ nAChRs in immature IHCs

Recent findings have shown that the current flowing through recombinant $\alpha9\alpha10$ nAChRs was potentiated by the divalent cations Ca^{2+} and Ba^{2+} at concentrations up to 500 μM and blocked at higher concentrations (Weisstaub *et al.* 2002). By contrast, the ACh-activated current through the homomeric $\alpha9$ receptor was reduced but not potentiated by Ca^{2+} regardless of the Ca^{2+} concentration (Katz *et al.* 2000). Therefore we investigated whether the native nAChRs expressed in immature IHCs showed biophysical properties of $\alpha9$ alone or of the heteromeric $\alpha9\alpha10$ receptors. To test the sensitivity of native nAChRs to extracellular Ca^{2+} we superfused apical IHCs ($n = 27$, P7) with a Ca^{2+}-free solution or with solutions containing 100 μM, 500 μM, 1 mM or 5 mM Ca^{2+}. The isolated ACh-activated currents (Fig. 8*A*), in the presence of different Ca^{2+} concentrations, were obtained by subtracting the control currents from the currents during the superfusion of ACh. As previously shown for the recombinant nAChRs (Weisstaub *et al.* 2002), extracellular Ca^{2+} concentrations up to 500 μM (Fig. 8*A*, top panels) increased both the instantaneous and steady-state inward nAChR currents, whereas a reduction occurred when higher concentrations of the ion were used (Fig. 8*A*, bottom panels). The remaining small current in the presence of a Ca^{2+}-free solution is likely to be carried by Na^+ flowing through nAChRs as previously described (McNiven *et al.* 1996; Weisstaub *et al.* 2002). Note the absence of outward SK current. A small ACh-activated current was also recorded when 5 mM Ca^{2+} was used as Ca^{2+} acts as a permeant blocker of heteromeric $\alpha9\alpha10$ nAChRs (Weisstaub *et al.* 2002). In this condition a small SK current was present. Single exponential fits to the current relaxation near −144 mV indicate that the time constant became significantly ($P < 0.0001$) faster as extracellular Ca^{2+} was increased (Ca^{2+}-Free: 29.6 ± 1.4 ms, $n = 5$; 100 μM: 21.9 ± 1.4 ms, $n = 8$; 500 μM: 18.3 ± 3.1 ms, $n = 5$; 1 mM: 10.7 ± 1.0 ms, $n = 5$; 5 mM: 1.1 ± 0.3 ms, $n = 4$). These results suggest that the observed current relaxation, at hyperpolarized test potentials, is likely to be due to extracellular Ca^{2+} partially blocking the nAChRs. The average instantaneous *I–V* curves for the different experimental conditions in Fig. 8*A* are shown in Fig. 8*B*.

Figure 8*C* shows the amplitude of the instantaneous inward current at a membrane potential near −144 mV as a function of extracellular Ca^{2+}, where both potentiating and blocking effects exerted by Ca^{2+} can be appreciated. The changes in current amplitude were significant at $P < 0.0001$. Both potentiation and block were also evident from the steady-state currents measured at the same potential (data not shown). In contrast to the inward nAChR current, the size of the instantaneous

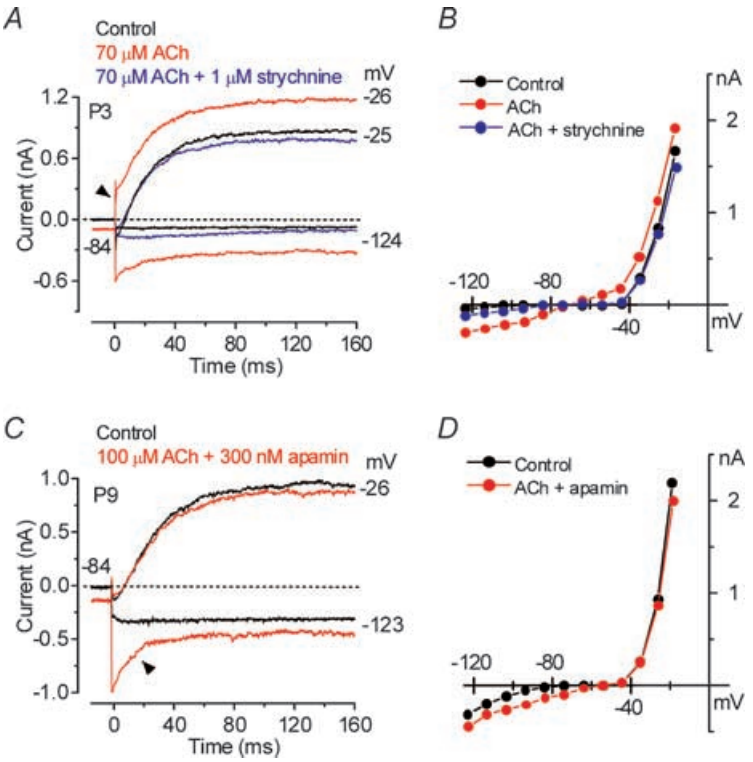

Figure 6. Strychnine and apamin affect the ACh-activated current in immature IHCs
A, current traces at nominal potentials of −24 and −124 mV before (control, black traces) and during superfusion of either 70 μM ACh alone (red traces) or together with 1 μM strychnine (blue traces). *B*, steady-state *I–V* curves for the three experimental conditions shown in *A*. P3: C_m 7.6 pF; R_s 1.4 MΩ; g_{leak} 1.1 nS. *C*, membrane currents obtained before (black traces) and during (red traces) superfusion of 100 μM ACh together with 300 nM apamin. Recording conditions as in *A*. *D*, steady-state *I–V* curves for the control current and the current recorded when both apamin and ACh were applied onto the cell shown in *C*. P9: C_m 9.0 pF; R_s 1.9 MΩ; g_{leak} 3.5 nS.

and steady-state outward current, mainly carried by the SK channel, was only significantly reduced ($P < 0.0001$) when extracellular Ca^{2+} was absent (Fig. 8*D*, for the instantaneous current). The similar sizes of the SK current over the range of 500 μM to 5 mM Ca^{2+} suggests that 500 μM Ca^{2+} is already sufficient for maximally activating the SK current. Increasing the extracellular Ca^{2+} concentration shifted ($P < 0.0001$) the reversal potential of the total ACh-activated current towards more hyperpolarized potentials (Fig. 8*E*), probably due to a progressively increased contribution from the SK current.

ACh modulates the action potential frequency of immature IHCs

An inhibitory role of ACh on evoked action potential activity has been reported for P7 rat IHCs (Glowatzki & Fuchs, 2000). To gain more insight into the modulation of the spontaneous and evoked action potential frequency by nAChRs, we investigated voltage responses before and during superfusion of different ACh concentrations in P2–P4 IHCs ($n = 32$), results for one of which are shown in Fig. 9*A–C*. The application of ACh onto IHCs at concentrations of 3 μM or 10 μM caused a hyperpolarizing shift in the resting potential and reduced the frequency of induced action potentials (Fig. 9*B*). Spontaneous spikes were abolished using 3 μM ACh, the lowest concentration tested. In the presence of 30 μM (Fig. 9*C*) or higher ACh concentrations, evoked spikes were abolished at all current injection levels tested (up to +220 pA) and the resting potential became progressively hyperpolarized. The effects of 10 μM ACh on action potentials were abolished when 100 nM strychnine was

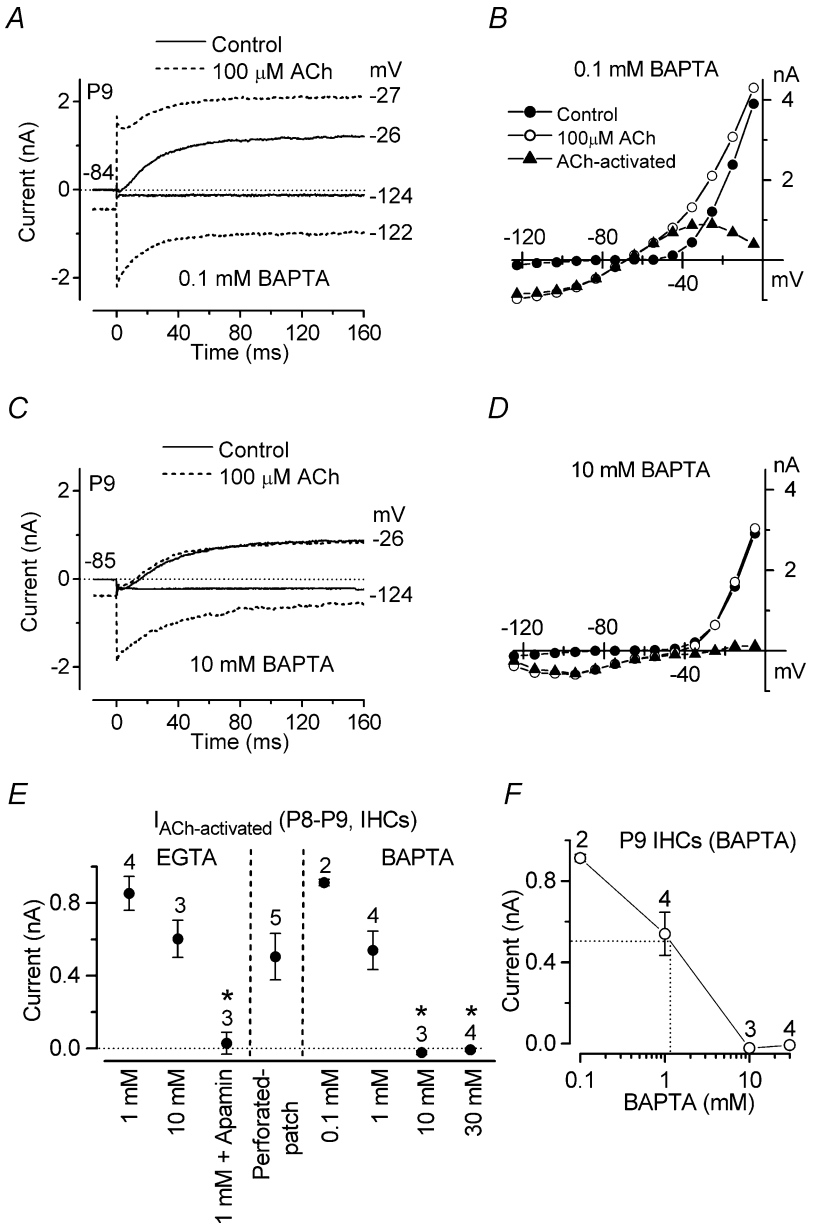

Figure 7. Effect of BAPTA on the ACh-activated SK current in immature IHCs
Membrane currents (*A* and *C*) and steady-state *I–V* curves (*B* and *D*) recorded in P9 apical IHCs before and during superfusion of 100 μM ACh when 0.1 mM (*A* and *B*) and 10 mM (*C* and *D*) BAPTA were used in the intracellular solution instead of 1 mM EGTA. 0.1 mM BAPTA: C_m 9.5 pF; R_s 1.5 MΩ; g_{leak} 1.0 nS. 10 mM BAPTA: C_m 9.6 pF; R_s 0.9 MΩ; g_{leak} 3.0 nS. *E*, steady-state amplitude (at 160 ms) measured near −26 mV for the current during the superfusion of 100 μM ACh minus the control current using different intracellular Ca^{2+} buffers and using perforated-patch recording. *F*, size of the ACh-activated outward K^+ current as a function of BAPTA concentration (data from *E*). The equivalent BAPTA concentration for the endogenous buffer is estimated by the dotted lines to be about 1 mM. All IHCs were from P8–P9 mice.

simultaneously superfused (Fig. 9*D*), providing support for the nicotinic nature of the AChRs. A similar effect of strychnine was also observed in seven other P2–P4 IHCs. The superfusion of strychnine alone did not affect the spike frequency when compared with control values ($n = 5$). Figure 9*E* shows that the reduction in spike frequency was dependent on both ACh concentration and the current injection amplitude. Increasing the extracellular concentration of ACh also resulted in a significant hyperpolarization ($P < 0.0001$) by up to −11 mV of the resting membrane potential (Fig. 9*F*) compared with that in control conditions (−62.2 ± 1.1 mV, $n = 32$, P2–P4).

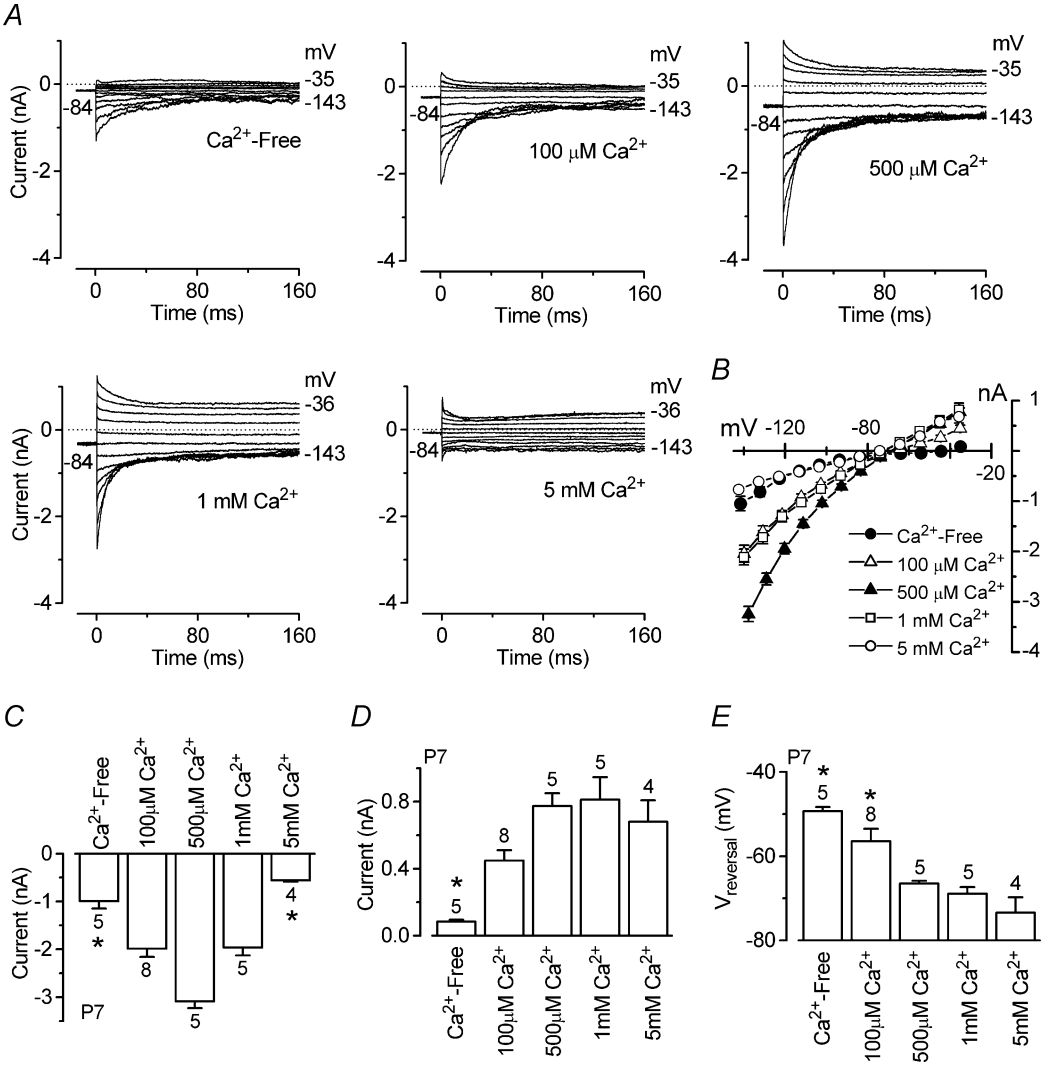

Figure 8. Extracellular Ca^{2+} both potentiates and blocks the ACh-activated current in immature IHCs
A, isolated ACh-activated currents (P7, apical IHCs) obtained by subtracting the control currents from the currents in the presence of 100 μM ACh when a Ca^{2+}-free solution or solutions containing different Ca^{2+} concentrations were superfused. All recordings were obtained using 0.9 mM extracellular Mg^{2+}. Currents were recorded in response to a series of voltage steps from −144 mV to more positive potentials in 10 mV nominal increments (160 ms in duration) from the holding potential of −84 mV. Dotted lines indicate zero current. Ca^{2+}-free (I_{hold} −145 pA) and 100 μM Ca^{2+} (I_{hold} −246 pA): C_m 8.6 pF; R_s 1.7 MΩ; g_{leak} 2.8 nS. 500 μM Ca^{2+} (I_{hold} −459 pA) and 1 mM Ca^{2+} (I_{hold} −316 pA): C_m 6.8 pF; R_s 1.5 MΩ; g_{leak} 1.2 nS. 5 mM Ca^{2+} (I_{hold} −71 pA): C_m 7.9 pF; R_s 2.0 MΩ; g_{leak} 1.5 nS. *B*, average instantaneous *I–V* curves for the ACh-activated currents in the presence of different Ca^{2+} concentrations including those in *A* (numbers of cells as in *C–E*). *C*, size of instantaneous inward currents measured near −144 mV. Note that the size of the currents in both the Ca^{2+}-free solution and the solution containing 5 mM Ca^{2+} was significantly smaller than that obtained in the presence of intermediate Ca^{2+} concentrations. *D*, size of instantaneous outward current measured around −35 mV. *E*, reversal potential of the instantaneous ACh-activated current as a function of extracellular Ca^{2+} concentration. Numbers of cells are shown above each column.

Effects of ACh on voltage responses in the absence of the SK current

As shown in Fig. 3*C–F* IHCs were unable to sustain repetitive action potentials when the SK current was blocked by apamin and the action potentials acquired long depolarized plateaus. Similar results were also obtained when 30 mM BAPTA was included in the intracellular solution (Fig. 10*A*) which prevents the activation of the SK current (Fig. 7*E*). In the presence of BAPTA, the application of 100 μM ACh (Fig. 10*B*) onto apical P6 IHCs now caused a depolarizing shift in the resting membrane potential (from -79.6 ± 1.5 to -48.2 ± 9.7 mV, $n = 4$, significant at $P < 0.05$) instead of the membrane hyperpolarization observed in Fig. 9*F* when the SK current was available. This depolarization led to a lowering of the threshold for firing action potentials with depolarized plateaus.

The role of ACh on IHC voltage responses was also investigated in five apical IHCs (P5–P7) when the SK channels were blocked by apamin. Since apamin eventually abolished repetitive action potential activity (Fig. 3*C–F*) we made use of the fact that it could not be completely removed from the preparation even after a long washout. Apamin (300 nM) was superfused onto IHCs until spontaneous or induced action potentials were abolished. Then the drug was washed out, using a normal extracellular solution, long enough for action potential activity to return (Fig. 10*C*, first 3 s of the voltage recording). Under these conditions, the superfusion of 100 μM ACh now caused the cells to depolarize (Fig. 10*C*) instead of hyperpolarize, probably due to a combination of cation current flowing through nAChRs and the partial block of the SK channels by the remaining apamin molecules. The effect of ACh was

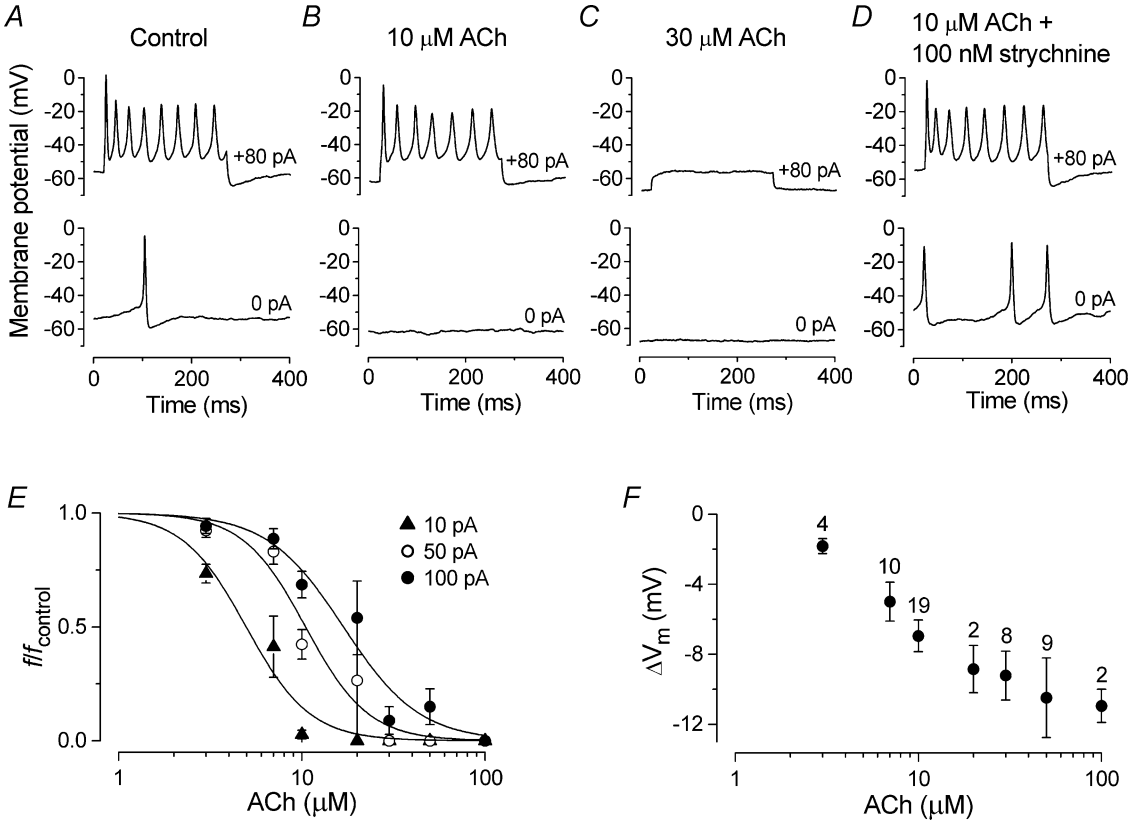

Figure 9. ACh reduces the frequency of action potentials in immature IHCs
A–D, voltage responses under current clamp from a P3 apical IHC recorded before (*A*) and during superfusion of ACh alone (*B* and *C*) or together with 100 nM strychnine (*D*). Current steps were applied from the resting potential in 10 pA increments between 0 pA and +100 pA and for clarity only a few traces are shown. C_m 8.5 pF; R_s 4.4 MΩ; g_{leak} 2.4 nS. *A*, V_m −53 mV: *B*, V_m −60 mV: *C*, V_m −67 mV: *D*, V_m −53 mV. *E*, reduction in spike frequency ($f/f_{control}$) caused by the superfusion of different concentrations of ACh (ranging from 3 to 100 μM) at three different current injection levels (10, 50 and 100 pA). Averaged data points from 32 P2–P4 apical-coil IHCs could be approximated using a logistic curve: $f/f_{control} = 1/(1 + ([D]/K_D)^{n_H})$, where $f/f_{control}$ is the normalized spike frequency and the other parameters are as described in the legend of Fig. 3*B*. 10 pA: $f_{control} = 9.4 \pm 0.8$ Hz, $K_D = 5.0$ μM; 50 pA: $f_{control} = 22.6 \pm 0.8$ Hz, $K_D = 10.5$ μM; 100 pA: $f_{control} = 28.3 \pm 0.7$ Hz, $K_D = 16.9$ μM. n_H was around 2.5 for all curves. *F*, changes in resting membrane potential (ΔV_m) as a function of ACh concentration. Number of measurements shown above averaged data points in *F* also apply to *E*. All recordings at body temperature.

partially reversible after washout (Fig. 10*C*, last 4 s of the recording).

Discussion

Identity of the Ca^{2+}-activated K^+ current in immature IHCs

Here we show that immature IHCs express a Ca^{2+}-activated K^+ current from just after birth that disappears after the onset of hearing. This transient expression suggests that this current might contribute, together with other currents (Marcotti *et al.* 1999, 2003*a*,*b*), to the maturation of IHCs. The novel current was still present when intracellular K^+ was substituted by Cs^+ (see Fig. 5*A* in Marcotti *et al.* 2003*b*) and was abolished during the superfusion of a Ca^+-free solution, nifedipine or the bee venom apamin. These results are consistent with the presence of an SK-type current (Sah & Faber, 2002) activated by Ca^{2+} influx into the cell through $Ca_v1.3$ voltage-gated Ca^{2+} channels known to be present in immature IHCs (Platzer *et al.* 2000; Marcotti *et al.* 2003*b*). An SK current was also isolated in OHCs from around the beginning of the second postnatal week, but contrary to IHCs its expression was not transient as it remained in adult cells. A current with pharmacological properties similar to those described above has also been reported in hair cells of various vertebrates (Fuchs & Murrow, 1992; Doi & Ohmori, 1993; Evans, 1996; Nenov *et al.* 1996*b*; Tucker & Fettiplace, 1996; Yamamoto *et al.* 1997; Yuhas & Fuchs, 1999).

The very low K_D for block by apamin (360 pM) in immature IHCs suggests that the most likely gene candidate responsible for the SK current is that expressing SK2 channels (Köhler *et al.* 1996). SK2 channels have been cloned from the mature mouse cochlea (Nie *et al.* 2004) and *in situ* hybridization and immunolabelling techniques have shown that in the mature rat cochlea these channels are expressed in OHCs but not in IHCs (Dulon *et al.* 1998; Oliver *et al.* 2000). The absence of mRNA encoding SK2 channels in mature IHCs (Dulon *et al.* 1998) is consistent with electrophysiological experiments showing the insensitivity of the total K^+ current to apamin (Kros & Crawford, 1990; Dulon *et al.* 1995; Marcotti *et al.* 2004).

Immature IHCs are transiently sensitive to the efferent neurotransmitter ACh

The SK channels expressed in hair cells are also thought to be activated by Ca^{2+} flowing through $\alpha9\alpha10$ nAChRs (Elgoyhen *et al.* 2001; Maison *et al.* 2002). The presence

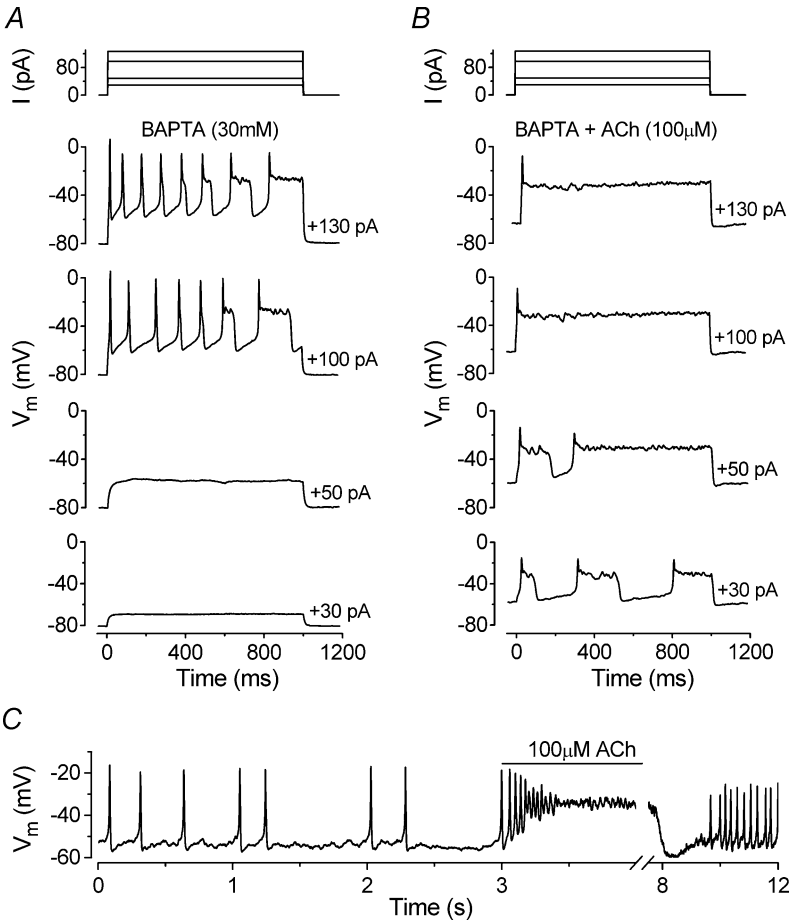

Figure 10. Effects of blocking the SK current on ACh-induced voltage responses in immature IHCs
A and *B*, voltage responses from a P6 apical IHC before and during superfusion of 100 μM ACh, respectively. The intracellular solution contained 30 mM BAPTA to prevent the activation of the SK current. Current steps were applied from the resting potential in 10 pA increments between 0 and +130 pA and for clarity only a few voltage responses are shown. Superfusion of ACh resulted in resting membrane potential depolarization from around −80 mV (*A*) to −60 mV (*B*). C_m 9.0 pF; R_s 7.1 MΩ. *C*, continuous voltage recording obtained by applying a 10 pA depolarizing current injection to an apical P5 IHC. Before the recording shown the cell was superfused with 300 nM apamin. The line above the voltage recording indicates the period of ACh application. Note the compressed time scale of the abscissa after the interruption. V_m −59 mV; C_m 7.1 pF; R_s 5.2 MΩ; g_{leak} 3.7 nS. All recordings at body temperature.

of heteromeric $\alpha9\alpha10$ nAChRs in immature IHCs was confirmed by experiments in which extracellular Ca^{2+} at micromolar concentrations potentiated and at millimolar concentrations reduced the ACh-activated current (Fig. 8), as previously described for the recombinant $\alpha9\alpha10$ nAChR (Weisstaub *et al.* 2002). Similar results, using a constant concentration of Mg^{2+}, have also been shown for native nAChRs in chick short hair cells (McNiven *et al.* 1996) and in a preliminary study on immature rat IHCs (Gómez-Casati *et al.* 2004). While the concentration-dependent block of the nAChR current (Fig. 8*A*) can be simply explained by Ca^{2+} acting as a permeant blocker of these receptors, the potentiation may be caused by Ca^{2+} enhancing the probability of the channel being open, as previously described in neurones (Mulle *et al.* 1992; Amador & Dani, 1995).

ACh is the main efferent neurotransmitter in the mammalian cochlea (Eybalin, 1993) and has been shown to affect hair cells of various vertebrates (Fuchs & Murrow, 1992; Doi & Ohmori, 1993; Dulon & Lenoir, 1996; Nenov *et al.* 1996*a*; Evans, 1996; Yamamoto *et al.* 1997; He & Dallos, 1999; Yuhas & Fuchs, 1999; Glowatzki & Fuchs, 2000). In the mouse, efferent fibres synapse directly with IHCs or with their afferents from around birth although some developmental variability exists between strains and cochlear regions (Sobkowicz, 1992; Bruce *et al.* 1997, 2000). At about the same time, ACh appears to be present in the efferent endings below IHCs (Sobkowicz & Emmerling, 1989; Merchan Perez *et al.* 1994). By about P12 axosomatic contact between efferent fibres and IHCs no longer occurs (Shnerson *et al.* 1982; Bruce *et al.* 2000). Consistent with these morphological observations our results show that apical IHCs respond to ACh from around P2 (Fig. 5*A*), matching the appearance of the SK current in these cells, until just after the onset of hearing. Although the slow activation time course of the SK current (Fig. 2*A–D*) is reminiscent of the $I_{K(Ca)}$ found in mature IHCs, the latter was insensitive to apamin and blocked by intracellular Cs^{+} which permeates through SK channels (Fig. 8 in Marcotti *et al.* 2004). Also, in the guinea-pig, apamin was ineffective in mature IHCs (Kros & Crawford, 1990; Dulon *et al.* 1995). These results suggest that the SK current is down-regulated in mature IHCs, perhaps simultaneously with the nAChRs.

The disappearance of ACh responses in mature IHCs is likely to be related to developmental changes in the expression of the nAChRs. The period during which mRNAs for heteromeric $\alpha9\alpha10$ nAChRs are present around the first 2 weeks of postnatal development (Morley & Simmons, 2002) coincides with the occurrence of axosomatic efferent innervation of IHCs and the cells responding to direct application of ACh. Interestingly, a low level of expression of $\alpha9$ mRNA alone in IHCs both before and after this period does not correlate with functional ACh receptors.

Contrary to IHCs, apical-coil OHCs begin to respond to ACh only from around the beginning of the second postnatal week (Fig. 5*B*), when the SK current was also detected for the first time in these cells in the absence of ACh. Previous studies on the rat and gerbil have shown that basal OHCs start to respond to ACh from P6 (Dulon & Lenoir, 1996; He & Dallos, 1999). Our findings are consistent with these results, considering that the maturation of apical OHCs is delayed by about 2 days compared with basal cells (He *et al.* 1994). The temporal discrepancy in the responsiveness to ACh between IHCs and OHCs is likely to be related to the later formation of efferent synaptic connections with OHCs (Pujol *et al.* 1998), which also corresponds to the expression of the heteromeric $\alpha9\alpha10$ nAChRs in these cells (Morley & Simmons, 2002).

Roles of the SK current and of efferent innervation in immature IHCs

Although it is known that efferent connections with OHCs reduce mechanical amplification in the mature cochlea (Guinan, 1996), their role in immature IHCs is less clear. Previous studies have shown that different current types expressed by immature IHCs can specifically modulate the shape and frequency of spontaneous or induced action potentials (Marcotti *et al.* 1999, 2003*a*,*b*). We were interested in determining whether the SK current has a well-defined role in modulating the action potentials in immature IHCs. Although these cells express both Ca^{2+} and Na^{+} currents, only the former is required for the generation of spontaneous and induced action potentials since they are reversibly abolished during superfusion of a Ca^{2+}-free solution but not by TTX (Marcotti *et al.* 2003*b*). While the Ca^{2+} current together with the K^{+} current $I_{K,neo}$ determines the rate of rise and fall and the amplitude of the spike (Fig. 11), the Na^{+} current reduces the interspike interval (Fig. 11 and Marcotti

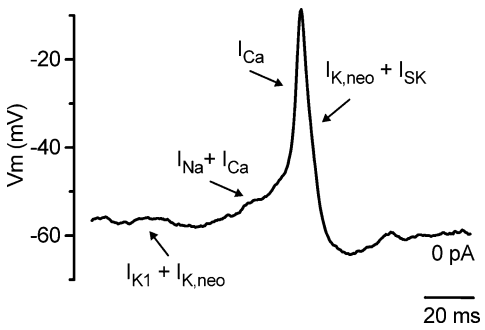

Figure 11. Role of different membrane currents in IHC action potential activity
Spontaneous action potential recorded from an apical coil IHC (P3). The different basolateral currents expressed in immature IHCs exert distinct roles in different phases of the action potentials, as indicated by the arrows. See discussion for details.

et al. 2003*b*). Finally, the resting membrane potential of immature IHCs is mainly determined by both $I_{K,neo}$ and the inward K^+ current I_{K1} (Fig. 11; Marcotti *et al.* 1999, 2003*a*). The increase in size of I_{K1} in the second postnatal week hyperpolarizes the resting potential and is the main factor in the disappearance of spontaneous, but not induced, action potentials from P6 onwards (Marcotti *et al.* 2003*a*).

Here we show that the SK current also plays a key role in the action potential activity, even in the absence of ACh. When the SK current was selectively abolished with apamin (Fig. 3*C*–*G*) or BAPTA (Fig. 10*A*) the repolarizing phase of the action potentials first became less efficient and eventually failed. By blocking the SK current the incomplete repolarization following each action potential would also cause a progressive inactivation of $I_{K,neo}$ (Marcotti *et al.* 2003*a*) and therefore reduce its contribution. These results indicate that the SK current, when activated by Ca^{2+} flowing through $Ca_v1.3$ Ca^{2+} channels, is essential for sustaining repetitive spikes in immature IHCs by making the repolarization phase of the action potentials more robust (Fig. 11). This role is in some respect different from that found in neurones, where the apamin-sensitive afterhyperpolarization (mAHP) mediated by SK channels does not contribute to the repolarization of the action potential itself but reduces the frequency of repetitive action potentials (Sah & Faber, 2002; Edgerton & Reinhart, 2003). The increase in action potential frequency in the presence of apamin (Fig. 3*C*) provides some evidence for the latter effect in IHCs as well. Since IHCs and OHCs exhibit otherwise qualitatively similar basolateral membrane currents (Marcotti & Kros, 1999; Marcotti *et al.* 1999, 2003*a*,*b*; Michna *et al.* 2003) it is possible that the lack of the SK current in immature OHCs is the crucial factor that prevents them firing repetitive action potentials (Marcotti & Kros, 1999).

In addition to this intrinsic spike modulation, IHCs can also be affected by efferent innervation due to the release of ACh and possibly various neuromodulators (Pujol *et al.* 1998). Although the SK current is normally involved in the repolarization phase of the action potential, the opening of nAChRs by ACh activates this current even at the resting membrane potential, causing IHCs to hyperpolarize (Fig. 9 and Glowatzki & Fuchs, 2000). As a consequence the spiking activity would be reduced or blocked, which in turn could affect the afferent discharge.

Both nAChRs and Ca^{2+} channels are closely coupled to SK channels in immature IHCs

We showed that SK channels are activated by a local increase in intracellular Ca^{2+} caused by the activation of voltage-gated Ca^{2+} channels and/or the opening of nAChRs. These separate sources of Ca^{2+} influx ensure a dual role for the SK channel in immature IHCs: in sustaining repetitive spiking activity and in mediating inhibitory efferent responses. However, Ca^{2+} influx into IHCs via voltage-gated Ca^{2+} channels also triggers neurotransmitter release at the afferent synapses (Beutner & Moser, 2001; Marcotti *et al.* 2003*b*). Since afferent and efferent fibres appear to be colocalized in immature IHCs (Shnerson *et al.* 1982; Bruce *et al.* 2000), the increase in intracellular Ca^{2+} caused by efferent stimulation could, at least in theory, also promote exocytosis. Therefore, to overcome cross-talk between efferent and afferent signalling the nAChRs and the synaptic ribbons need to be separated both spatially and by efficient Ca^{2+} buffering, possibly by calretinin and/or parvalbumin (Dechesne *et al.* 1994; Hackney *et al.* 2003).

Information about the colocalization between SK channels and both Ca^{2+} channels and nAChRs was gained from experiments in which the SK current was recorded in the presence of intracellular BAPTA (Figs 2*C*, *E* and *F* and 7). Although BAPTA and EGTA have similar affinities for Ca^{2+}, BAPTA has a much higher binding rate constant (Naraghi & Neher, 1997) enabling it to buffer increases in intracellular Ca^{2+} closer to its source (Neher, 1998). Our results show that SK channels were effectively uncoupled from the Ca^{2+} channels (Fig. 2*E*) and nAChRs (Fig. 7*E*) when 1 and 10 mM BAPTA were used, respectively. From Naraghi & Neher's (1997) estimate of 28 nm for the length constant for 2 mM BAPTA, the length constant for 1 mM and 10 mM BAPTA would differ by about $\sqrt{2}$ and $\sqrt{0.2}$, respectively (see eqn (2) in Neher, 1998). Therefore, we estimate that while Ca^{2+} channels are likely to be localized in the order of 40 nm away from the SK channels the nAChRs would be closer at about 13 nm. The latter estimate is in good agreement with a previous suggestion of some 10 nm for the distance between SK channels and nAChRs in rat OHCs (Oliver *et al.* 2000). Assuming that the Ca^{2+} channels are colocalized with the synaptic ribbons in hotspots (Tucker & Fettiplace, 1995; Zenisek *et al.* 2003) this provides evidence that the afferent and efferent nerve endings are indeed spatially separated in immature IHCs. The slow activation of the SK current in response to Ca^{2+} entry through the $Ca_v1.3$ Ca^{2+} channels (Figs 1 and 2*A* and *B*) suggests effective cytoplasmic buffering between the two types of nerve endings.

The question is whether both $Ca_v1.3$ Ca^{2+} channels and nAChRs are involved in the activation of the SK current under physiological conditions in which endogenous Ca^{2+} buffering is retained. The concentration of the mobile Ca^{2+} buffer in immature IHCs was estimated around 1 mM (Figs 2*F* and 7*F*), similar to that previously found in turtle auditory (Tucker & Fettiplace, 1996; Ricci *et al.* 2000) and frog saccular (Roberts, 1993) hair cells, suggesting that both mechanisms could indeed contribute significantly to the activation of the SK current *in vivo*.

References

Amador M & Dani JA (1995). Mechanism for modulation of nicotinic acetylcholine receptors that can influence synaptic transmission. *J Neurosci* **15**, 4525–4532.

Beutner D & Moser T (2001). The presynaptic function of mouse cochlear inner hair cells during development of hearing. *J Neurosci* **21**, 4593–4599.

Blaustein MP & Goldman DE (1968). The action of certain polyvalent cations on the voltage-clamped Lobster axon. *J General Physiol* **51**, 279–291.

Bruce LL, Christensen MA & Warr WB (2000). Postnatal development of efferent synapses in the rat cochlea. *J Comp Neurol* **423**, 532–548.

Bruce LL, Kingsley J, Nichols DH & Fritzsch B (1997). The development of vestibulocochlear efferents and cochlear afferents in mice. *Int J Dev Neurosci* **15**, 671–692.

Dechesne CJ, Rabejac D & Desmadryl G (1994). Development of calretinin immunoreactivity in the mouse inner ear. *J Comp Neurol* **346**, 517–529.

Doi T & Ohmori H (1993). Acetylcholine increases intracellular Ca^{2+} concentration and hyperpolarizes the guinea-pig outer hair cell. *Hear Res* **67**, 179–188.

Dulon D & Lenoir M (1996). Cholinergic responses in developing outer hair cells of the rat cochlea. *Eur J Neurosci* **8**, 1945–1952.

Dulon D, Luo L, Zhang C & Ryan AF (1998). Expression of small-conductance calcium-activated potassium channels (SK) in outer hair cells of the rat cochlea. *Eur J Neurosci* **10**, 907–915.

Dulon D, Sugasawa M, Blanchet C & Erostegui C (1995). Direct measurements of Ca^{2+}-activated K^+ currents in inner hair cells of the guinea-pig cochlea using photolabile Ca^{2+} chelators. *Pflugers Arch* **430**, 365–373.

Edgerton JR & Reinhart PH (2003). Distinct contributions of small and large conductance Ca^{2+}-activated K^+ channels to rat Purkinje neuron function. *J Physiol* **548**, 53–69.

Ehret G (1975). Masked auditory thresholds, critical ratios, and scales of the basilar membrane of the housemouse (*Mus musculus*). *J Comp Physiol* **103**, 329–341.

Elgoyhen AB, Johnson DS, Boulter J, Vetter DE & Heinemann S (1994). Alpha 9: an acetylcholine receptor with novel pharmacological properties expressed in rat cochlear hair cells. *Cell* **79**, 705–715.

Elgoyhen AB, Vetter DE, Katz E, Rothlin CV, Heinemann SF & Boulter J (2001). alpha10: a determinant of nicotinic cholinergic receptor function in mammalian vestibular and cochlear mechanosensory hair cells. *Proc Natl Acad Sci U S A* **98**, 3501–3506.

Evans MG (1996). Acetylcholine activates two currents in guinea-pig outer hair cells. *J Physiol* **491**, 563–578.

Eybalin M (1993). Neurotransmitters and neuromodulators of the mammalian cochlea. *Physiol Rev* **73**, 309–373.

Fuchs PA & Murrow BW (1992). Cholinergic inhibition of short (outer) hair cells of the chick's cochlea. *J Neurosci* **12**, 800–809.

Gil-Loyzaga PE (1995). Neurotransmitters of the olivocochlear lateral efferent system: with an emphasis on dopamine. *Acta Otolaryngol* **115**, 222–226.

Glowatzki E & Fuchs PA (2000). Cholinergic synaptic inhibition of inner hair cells in the neonatal mammalian cochlea. *Science* **288**, 2366–2368.

Gómez-Casati ME, Fuchs PA, Elgoyhen AB & Katz E (2004). Ca^{2+} modulates nicotinic ACh receptors of inner hair cells in the neonatal rat cochlea. 27th *ARO Midwinter Meeting*, 717*P*.

Guinan JJ Jr (1996). Physiology of olivocochlear efferents. In *The Cochlea*, ed. Dallos P, Popper AN, Fay RR, pp. 435–502. Springer, New York.

Guth PS & Norris CH (1996). The hair cell acetylcholine receptors: a synthesis. *Hear Res* **98**, 1–8.

Hackney CM, Mahendrasingam S, Jones EM & Fettiplace R (2003). The distribution of calcium buffering proteins in the turtle cochlea. *J Neurosci* **23**, 457745–457789.

He DZ & Dallos P (1999). Development of acetylcholine-induced responses in neonatal gerbil outer hair cells. *J Neurophysiol* **81**, 1162–1170.

He DZ, Evans BN & Dallos P (1994). First appearance and development of electromotility in neonatal gerbil outer hair cells. *Hear Res* **78**, 77–90.

Holt JC, Lioudyno M & Guth PS (2003). A pharmacologically distinct nicotinic ACh receptor is found in a subset of frog semicircular canal hair cells. *J Neurophysiol* **90**, 1526–1536.

Housley GD, Greenwood D & Ashmore JF (1992). Localization of cholinergic and purinergic receptors on outer hair cells isolated from the guinea-pig cochlea. *Proc R Soc Lond* B *Biol Sci* **249**, 265–273.

Katz E, Verbitsky M, Rothlin CV, Vetter DE, Heinemann SF & Elgoyhen AB (2000). High calcium permeability and calcium block of the alpha9 nicotinic acetylcholine receptor. *Hear Res* **141**, 117–128.

Köhler M, Hirschberg B, Bond CT, Kinzie JM, Marrion NV, Maylie J & Adelman JP (1996). Small-conductance, calcium-activated potassium channels from mammalian brain. *Science* **273**, 1709–1714.

Kros CJ & Crawford AC (1990). Potassium currents in inner hair cells isolated from the guinea-pig cochlea. *J Physiol* **421**, 263–291.

Kros CJ, Ruppersberg JP & Rüsch A (1998). Expression of a potassium current in inner hair cells during development of hearing in mice. *Nature* **394**, 281–284.

McNiven AI, Yuhas WA & Fuchs PA (1996). Ionic dependence and agonist preference of an acetylcholine receptor in hair cells. *Audit Neurosci* **2**, 63–77.

Maffei L & Galli-Resta L (1990). Correlation in the discharges of neighboring rat retinal ganglion cells during prenatal life. *Proc Natl Acad Sci U S A* **87**, 2861–2864.

Maison SF, Luebke AE, Liberman MC & Zuo J (2002). Efferent protection from acoustic injury is mediated via alpha9 nicotinic acetylcholine receptors on outer hair cells. *J Neurosci* **22**, 10838–10846.

Marcotti W, Géléoc GSG, Lennan GWT & Kros CJ (1999). Developmental expression of an inwardly rectifying potassium conductance in inner and outer hair cells along the mouse cochlea. *Pflugers Arch* **439**, 113–122.

Marcotti W, Johnson SL, Holley MC & Kros CJ (2003*a*). Developmental changes in the expression of potassium currents of embryonic, neonatal and mature mouse inner hair cells. *J Physiol* **548**, 383–400.

Marcotti W, Johnson SL & Kros CJ (2004). Effects of intracellular stores and extracellular Ca^{2+} on Ca^{2+}-activated K^+ currents in mature mouse inner hair cells. *J Physiol* **557**, 613–633.

Marcotti W, Johnson SL, Rüsch A & Kros CJ (2003*b*). Sodium and calcium currents shape action potentials in immature mouse inner hair cells. *J Physiol* **552**, 743–761.

Marcotti W & Kros CJ (1999). Developmental expression of the potassium current $I_{K,n}$ contributes to maturation of mouse outer hair cells. *J Physiol* **520**, 653–660.

Meister M, Wong RO, Baylor DA & Shatz CJ (1991). Synchronous bursts of action potentials in ganglion cells of the developing mammalian retina. *Science* **252**, 939–943.

Merchan Perez A, Gil-Loyzaga P, Eybalin M, Fernandez Mateos P & Bartolome MV (1994). Choline-acetyltransferase-like immunoreactivity in the organ of Corti of the rat during postnatal development. *Brain Res Dev Brain Res* **82**, 29–34.

Michna M, Knirsch M, Hoda J-C, Muenkner S, Langer P, Platzer J, Striessnig J & Engel J (2003). Cav1.3 (α1D) Ca^{2+} currents in neonatal outer hair cells of mice. *J Physiol* **553**, 747–758.

Morley BJ & Simmons DD (2002). Developmental mRNA expression of the alpha10 nicotinic acetylcholine receptor subunit in the rat cochlea. *Brain Res Dev Brain Res* **139**, 87–96.

Mulle C, Lena C & Changeux JP (1992). Potentiation of nicotinic receptor response by external calcium in rat central neurons. *Neuron* **8**, 937–945.

Naraghi M & Neher E (1997). Linearized buffered Ca^{2+} diffusion in microdomains and its implications for calculation of $[Ca^{2+}]$ at the mouth of a calcium channel. *J Neurosci* **17**, 6961–6973.

Neher E (1998). Vesicle pools and Ca^{2+} microdomains: new tools for understanding their roles in neurotransmitter release. *Neuron* **20**, 389–399.

Nenov AP, Norris C & Bobbin RP (1996*a*). Acetylcholine response in guinea pig outer hair cells. I. Properties of the response. *Hear Res* **101**, 132–148.

Nenov AP, Norris C & Bobbin RP (1996*b*). Acetylcholine response in guinea pig outer hair cells. II. Activation of a small conductance Ca^{2+}-activated K^+ channel. *Hear Res* **101**, 149–172.

Nie L, Song H, Cheng M, Chiamvimonvat N, Beisel KW, Yamoah EN & Vazquez AE (2004). Cloning and expression of a small conductance Ca^{2+}-activated K^+ channel from the mouse cochlea: coexpression with α9/α10 acetylcholine receptors. *J Neurophysiol* **91**, 1536–1544.

Oliva C, Cohen IS & Mathias RT (1988). Calculation of time constants for intracellular diffusion in whole cell patch clamp configuration. *Biophys J* **54**, 791–799.

Oliver D, Klocker N, Schuck J, Baukrowitz T, Ruppersberg JP & Fakler B (2000). Gating of Ca^{2+}-activated K^+ channels controls fast inhibitory synaptic transmission at auditory outer hair cells. *Neuron* **26**, 595–601.

Platzer J, Engel J, Schrott-Fischer A, Stephan K, Bova S, Chen H, Zheng H & Striessnig J (2000). Congenital deafness and sinoatrial node dysfunction in mice lacking class D L-type Ca^{2+} channels. *Cell* **102**, 89–97.

Pujol R, Lavigne-Rebillard M & Lenoir M (1998). Development of sensory and neural structures in the mammalian cochlea. In *Development of the Auditory System*, ed. Rubel EW, Popper AN & Fay RR, pp. 146–192. Springer, New York.

Rae J, Cooper K, Gates P & Watsky M (1991). Low access resistance perforated patch recordings using amphotericin B. *J Neurosci Meth* **37**, 15–26.

Ricci AJ, Gray-Keller M & Fettiplace R (2000). Tonotopic variations of calcium signalling in turtle auditory hair cells. *J Physiol* **524**, 423–436.

Roberts WM (1993). Spatial calcium buffering in saccular hair cells. *Nature* **363**, 74–76.

Sah P & Faber ES (2002). Channels underlying neuronal calcium-activated potassium currents. *Prog Neurobiol* B, 345–353.

Shatz CJ & Stryker MP (1988). Prenatal tetrodotoxin infusion blocks segregation of retinogeniculate afferents. *Science* **242**, 87–89.

Shnerson A, Devigne C & Pujol R (1982). Age-related changes in the C57BL/6J mouse cochlea. II. Ultrastructural findings. *Dev Brain Res* **2**, 77–88.

Sobkowicz HM (1992). The development of innervation in the organ of Corti. In *Development of Auditory and Vestibular Systems 2*, ed. Romand R, pp. 59–100. Elsevier, Amsterdam.

Sobkowicz HM & Emmerling MR (1989). Development of acetylcholinesterase-positive neuronal pathways in the cochlea of the mouse. *J Neurocytol* **18**, 209–224.

Tucker TR & Fettiplace R (1995). Confocal imaging of calcium microdomains and calcium extrusion in turtle hair cells. *Neuron* **15**, 1323–1335.

Tucker TR & Fettiplace R (1996). Monitoring calcium in turtle hair cells with a calcium-activated potassium channel. *J Physiol* **494**, 613–626.

Uziel A, Romand R & Marot M (1981). Development of cochlear potentials in rats. *Audiology* **20**, 89–100.

Weisstaub N, Vetter DE, Elgoyhen AB & Katz E (2002). The alpha9alpha10 nicotinic acetylcholine receptor is permeable to and is modulated by divalent cations. *Hear Res* **167**, 122–135.

Xia XM, Fakler B, Rivard A, Wayman G, Johnson-Pais T, Keen JE, Ishii T, Hirschberg B, Bond CT, Lutsenko S, Maylie J & Adelman JP (1998). Mechanism of calcium gating in small-conductance calcium-activated potassium channels. *Nature* **395**, 503–507.

Yamamoto T, Kakehata S, Yamada T, Saito T, Saito H & Akaike N (1997). Effects of potassium channel blockers on the acetylcholine-induced currents in dissociated outer hair cells of guinea pig cochlea. *Neurosci Lett* **236**, 79–82.

Yuhas WA & Fuchs PA (1999). Apamin-sensitive, small-conductance, calcium-activated potassium channels mediate cholinergic inhibition of chick auditory hair cells. *J Comp Physiol* **185**, 455–462.

Zenisek D, Davila V, Wan L & Almers W (2003). Imaging calcium entry sites and ribbon structures in two presynaptic cells. *J Neurosci* **23**, 2538–2548.

Acknowledgements

This work was supported by the MRC.